arXiv:1611.06479v1 [cond-mat.str-el] 20 Nov 2016

Emergence of an excitonic collective mode in the dilute electron gas

Yasutami Takada*

Institute for Solid State Physics, University of Tokyo, Kashiwa, Chiba 277-8581, Japan

(Dated: November 22, 2016)

By comparing two expressions for the polarization function $\Pi(\boldsymbol{q}, i\omega)$ given in terms of two different local-field factors, $G_+(\boldsymbol{q}, i\omega)$ and $G_s(\boldsymbol{q}, i\omega)$, we have derived the kinetic-energy-fluctuation (or sixth-power) sum rule for the momentum distribution function $n(\boldsymbol{p})$ in the three-dimensional electron gas. With use of this sum rule, together with the total-number (or second-power) and the kinetic-energy (or fourth-power) sum rules, we have obtained $n(\boldsymbol{p})$ in the low-density electron gas at negative compressibility (namely, $r_s > 5.25$ with r_s being the conventional density parameter) up to $r_s \approx 22$ by improving on the interpolation scheme due to Gori-Giorge and Ziesche proposed in 2002. The obtained results for $n(\boldsymbol{p})$ combined with the improved form for $G_s(\boldsymbol{q}, \omega + i0^+)$ are employed to calculate the dynamical structure factor $S(\boldsymbol{q}, \omega)$ to reveal that a giant peak, even bigger than the plasmon peak, originating from an excitonic collective mode made of electron-hole pair excitations, emerges in the low-ω region at $|\boldsymbol{q}|$ near $2p_{\rm F}$ ($p_{\rm F}$: the Fermi wave number). Connected with this mode, we have discovered a singular point in the retarded dielectric function at $\omega = 0$ and $|\boldsymbol{q}| \approx 2p_{\rm F}$.

PACS numbers: 71.10.Ca, 71.45.Gm, 05.30.Fk, 71.10.Hf

I. INTRODUCTION

The electron gas, an assembly of N electrons embedded in a uniform positive rigid background, has been investigated for a very long time, not only because it is relevant in understanding the exchange-correlation effects in simple metals and semiconductors, but also because it provides indispensable information for the actual implementation of the density functional theory (DFT), especially in its local density approximation (LDA).[1]

From a physical point of view, we may claim that this system is even more important in the low-density regime (namely, $p_{\rm F}a_0 \ll 1$ with $p_{\rm F}$ the Fermi wave number and a_0 the lattice constant), because in this regime the first-principles Hamiltonian to describe conduction electrons in a metal is universally reduced to the one for the electron gas, leading us to recognize that understanding the physical properties of the dilute electron gas is nothing but revealing the *universal* electron-correlation behavior of actual dilute metals.

The dilute electron gas, however, is not well understood; the thermodynamic quantities, such as the correlation energy ε_c and the compressibility κ, are accurately obtained as a function of the density parameter r_s by the Green's-Function Monte Carlo (GFMC) method[2] and the interpolation formulas to reproduce the GFMC data[3,4], where r_s is defined by $r_s = (4\pi n/3)^{-1/3}/a_B = (\alpha p_{\rm F} a_B)^{-1}$ with $n = N/\Omega_t$ the electron density, Ω_t the total volume of the system, $\alpha = (4/9\pi)^{1/3} \approx 0.5211$ and a_B the Bohr radius. The diffusion Monte Carlo (DMC) calculations are done to analyze the ground-state phases, including spin polarization, in the wide range of r_s[5] and recently for $0.5 \le r_s \le 20$ in more detail[6], but we do not know the precise behavior of other physical quantities, such as the momentum distribution function $n(\boldsymbol{p})$ for $r_s > 5$. It is true that some quantum Monte Carlo calculations are done to obtain $n(\boldsymbol{p})$ for $r_s \le 10$,[7,8] but the results are not very accurate due probably to large size effects and improper starting trial functions, judging from the assessment of their accuracy by the sum rules for $n(\boldsymbol{p})$.[9,10] As for the dynamical structure factor $S(\boldsymbol{q}, \omega)$, no reliable data are available in the dilute metallic regime.

One of the characteristic features of the dilute electron gas is the appearance of "dielectric catastrophe" associated with the divergence of κ at $r_s = r_s^c \equiv 5.25$ followed by negative κ for $r_s > r_s^c$,[11,12] implying that the static polarization function $\Pi(\boldsymbol{q}, 0)$ in the long wave-length limit is also *negative* (and thus dielectrically anomalous) owing to the compressibility sum rule, $\lim_{|\boldsymbol{q}|\to 0} \Pi(\boldsymbol{q}, 0) = n^2\kappa\Omega_t$.[13] This anomaly for $r_s > r_s^c$ brings about the curious behavior of the ion-ion pair correlation function in expanded liquid alkali metals,[14–16] but it does not induce any instabilities in the electron gas itself, as long as $1/\kappa$ changes continuously from positive to negative through the point of $1/\kappa = 0$,[17] because the electron-electron effective interaction is not determined only by the dielectric function $\varepsilon(\boldsymbol{q}, i\omega) = 1 + V(\boldsymbol{q})\Pi(\boldsymbol{q}, i\omega)$ with $V(\boldsymbol{q}) = 4\pi e^2/(\Omega_t \boldsymbol{q}^2)$ the bare Coulomb interaction,[18] excluding the occurrence of CDW-type instabilities at $r_s = r_s^c$.[19]

By analyzing $\varepsilon^R(\boldsymbol{q}, \omega)[= \varepsilon(\boldsymbol{q}, \omega + i0^+)]$ the retarded dielectric function as r_s approaches r_s^c from the positive side of κ (or $r_s < r_s^c$), we identify the physical origin of this divergence of κ as the "enhanced excitonic effect" or the effect of strong electron-hole attraction in an electron-hole single-pair excitation.[20] For $r_s > r_s^c$, by considering causality, Takayanagi and Lipparini[21] conclude that $\Pi(\boldsymbol{q}, i\omega)$ contains an anomalous part $\Pi_a(\boldsymbol{q}, i\omega)$ made of a single pair of poles at $i\omega = \pm i\tilde{\omega}_{\rm ex}(\boldsymbol{q})$ in the form of

$$\Pi_a(\boldsymbol{q}, i\omega) = \frac{1}{V(\boldsymbol{q})} \frac{ne^2}{m} \frac{f_{\rm ex}(\boldsymbol{q})}{\omega^2 - \tilde{\omega}_{\rm ex}(\boldsymbol{q})^2}, \tag{1}$$

with m the mass of a free electron. These poles at which $\Pi(\boldsymbol{q}, i\omega)$ diverges, however, do not give any prominent structures in the observable physical quantity $S(\boldsymbol{q}, \omega)$,

which can be calculated by $S(\boldsymbol{q},\omega) = -\mathrm{Im}Q_c^R(\boldsymbol{q},\omega)/\pi$ for $\omega > 0$ at zero temperature ($T = 0$) with the retarded charge response function $Q_c^R(\boldsymbol{q},\omega)$, given by

$$Q_c^R(\boldsymbol{q},\omega) = -\frac{\Pi(\boldsymbol{q},\omega+i0^+)}{1+V(\boldsymbol{q})\Pi(\boldsymbol{q},\omega+i0^+)}. \tag{2}$$

Then a couple of questions arise: what is the physical role of these poles and how the strong excitonic effect manifests itself in $S(\boldsymbol{q},\omega)$ for $r_s > r_s^c$? We shall address these questions by accurately determining $\tilde{\omega}_{\rm ex}(\boldsymbol{q})$, "the oscillator strength" of the pole $f_{\rm ex}(\boldsymbol{q})$, and $S(\boldsymbol{q},\omega)$ for r_s from r_s^c up to about 20 in which the ground state has already been confirmed to be a paramagnetic metal.[6]

A straightforward way of obtaining accurate results for $S(\boldsymbol{q},\omega)$ is to perform the highly self-consistent calculation in the GWΓ scheme[22] which includes the vertex function Γ satisfying the Ward identity (WI),[23,24] just as done for $S(\boldsymbol{q},\omega)$ for $r_s \le 5$,[25] but it turns out that this GWΓ does not work well in the dielectric-catastrophe regime. Thus it is revised into the $\mathrm{G\tilde{W}\tilde{\Gamma}_{WI}}$ scheme[10,26] to obtain the self-consistent results for $S(\boldsymbol{q},\omega)$ as well as $n(\boldsymbol{p})$ up to $r_s = 10$, but there still remains the problem of reaching a fully self-consistent solution for $r_s > 10$.

Confronted with this difficulty, we will take the following strategy; firstly, we reconsider the parametrization scheme for determining $n(\boldsymbol{p})$ due to Gori-Giorgi and Ziesche (GZ),[27] who interpolate the accurate data for $n(\boldsymbol{p})$ in the effective potential expansion (EPX) method[9] for $1 \le r_s \le 5$ with that in the Wigner-crystal limit ($r_s \gg 10$), together with the two sum rules, one for the total number and the other for the total kinetic energy,[9] expressed as

$$\sum_{\boldsymbol{p}\sigma} n(\boldsymbol{p}) = N, \tag{3}$$

$$\sum_{\boldsymbol{p}\sigma} \varepsilon_{\boldsymbol{p}} n(\boldsymbol{p}) = N\langle\varepsilon_{\boldsymbol{p}}\rangle = N\left(\frac{3}{5}E_{\rm F} - \varepsilon_c - r_s\frac{\partial\varepsilon_c}{\partial r_s}\right), \tag{4}$$

with σ the spin variable, $\varepsilon_{\boldsymbol{p}} = \boldsymbol{p}^2/2m$, and $E_{\rm F} = p_{\rm F}^2/2m$ the Fermi energy. This GZ scheme can give rather accurate $n(\boldsymbol{p})$ for $r_s \lesssim 12$. Here we shall improve on it by increasing the number of input data for $n(\boldsymbol{p})$ that we obtain up to $r_s = 10$ in $\mathrm{G\tilde{W}\tilde{\Gamma}_{WI}}$. We also use, in addition to the above two, the third sum rule for the total kinetic-energy fluctuation, written as

$$\sum_{\boldsymbol{p}\sigma} \varepsilon_{\boldsymbol{p}}^2 n(\boldsymbol{p}) = N\left[\langle(\varepsilon_{\boldsymbol{p}} - \langle\varepsilon_{\boldsymbol{p}}\rangle)^2\rangle + \langle\varepsilon_{\boldsymbol{p}}\rangle^2\right]. \tag{5}$$

We shall derive this sum rule in Sec. II with giving a concrete value for the righthand side of Eq. (5).

Secondly, once $n(\boldsymbol{p})$ is known, we can calculate $\Pi(\boldsymbol{q},i\omega)$ by the formula given in $\mathrm{G\tilde{W}\tilde{\Gamma}_{WI}}$ as

$$\Pi(\boldsymbol{q},i\omega) = \frac{\Pi_{\rm WI}(\boldsymbol{q},i\omega)}{1 - V(\boldsymbol{q})G_s(\boldsymbol{q},i\omega)\Pi_{\rm WI}(\boldsymbol{q},i\omega)}, \tag{6}$$

where $\Pi_{\rm WI}(\boldsymbol{q},i\omega)$ is defined as

$$\Pi_{\rm WI}(\boldsymbol{q},i\omega) = \sum_{\boldsymbol{p}\sigma}\frac{n(\boldsymbol{p}+\boldsymbol{q}) - n(\boldsymbol{p})}{i\omega - \varepsilon_{\boldsymbol{p}+\boldsymbol{q}} + \varepsilon_{\boldsymbol{p}}}, \tag{7}$$

with $G_s(\boldsymbol{q},i\omega)$ the local-field factor as introduced by Richardson and Ashcroft.[28] This factor is different from the conventinal local-field factor $G_+(\boldsymbol{q},i\omega)$,[18] with which $\Pi(\boldsymbol{q},i\omega)$ is expressed in another way as

$$\Pi(\boldsymbol{q},i\omega) = \frac{\Pi_0(\boldsymbol{q},i\omega)}{1 - V(\boldsymbol{q})G_+(\boldsymbol{q},i\omega)\Pi_0(\boldsymbol{q},i\omega)}, \tag{8}$$

with $\Pi_0(\boldsymbol{q},i\omega)$ the Lindhard function, given by

$$\Pi_0(\boldsymbol{q},i\omega) = \sum_{\boldsymbol{p}\sigma}\frac{n_0(\boldsymbol{p}+\boldsymbol{q}) - n_0(\boldsymbol{p})}{i\omega - \varepsilon_{\boldsymbol{p}+\boldsymbol{q}} + \varepsilon_{\boldsymbol{p}}}, \tag{9}$$

with $n_0(\boldsymbol{p}) = \theta(p_{\rm F} - |\boldsymbol{p}|)$ the step function. The obtained $\Pi(\boldsymbol{q},i\omega)$ can be used to determine both $\tilde{\omega}_{\rm ex}(\boldsymbol{q})$ and $f_{\rm ex}(\boldsymbol{q})$ by the analysis of its divergent property.

Finally, we need to make an analytic continuation of $\Pi(\boldsymbol{q},i\omega)$ into $\Pi(\boldsymbol{q},\omega+i0^+)$ to calculate $S(\boldsymbol{q},\omega)$. There are two ingredients, $\Pi_{\rm WI}(\boldsymbol{q},\omega+i0^+)$ and $G_s(\boldsymbol{q},\omega+i0^+)$, in this analytic continuation. The former can be obtained by the direct calculation through Eq. (7) with $\omega+i0^+$ in place of $i\omega$. As for the latter, we find it better to slightly modify $G_s(\boldsymbol{q},i\omega)$ from the original form[28], so that we can not only obtain much more accurate ε_c in a wide range of r_s by the adiabatic connection formula[29] but also eliminate unphysical divergences from $G_s(\boldsymbol{q},\omega+i0^+)$.

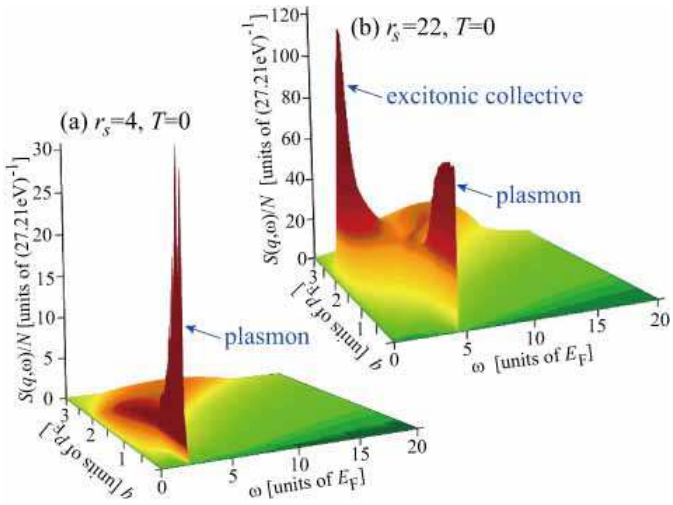

FIG. 1: (Color online) Bird's-eye view of $S(\boldsymbol{q},\omega)$ in the electron gas at zero temperature at (a) a usual metallic density $r_s = 4$, in which the plasmon peak dominates, and (b) a very dilute density $r_s = 22$, in which an excitonic collective peak, much bigger than the plasmon peak, emerges.

In accordance with the above strategy, we have successfully performed the calculation and obtained the results of both $n(\boldsymbol{p})$ and $S(\boldsymbol{q},\omega)$ for r_s up to over 20 to reveal that a giant peak other than the conventional plasmon one emerges in $S(\boldsymbol{q},\omega)$ for $r_s \gtrsim 10$, evolving into a predominant peak for $r_s > 20$, as shown in Fig. 1. Concomitantly a singular behavior is found in $n(\boldsymbol{p})$ for

$r_s \gtrsim 22$, which might suggest the occurrence of an electronic phase transition, though at present we cannot draw a definite conclusion on this point. Because the new peak in $S(\boldsymbol{q},\omega)$ is evolved from the shoulder structure due to the excitonic effect found at usual metallic densities[25], this peak may be called "an excitonic collective mode", a new concept in the dilute electron gas. In the dielectric-catastrophe regime, we also find that $\varepsilon^R(\boldsymbol{q},\omega)$ is controlled by the value of $\boldsymbol{q}_{\rm ex}(\neq \boldsymbol{0})$ at which $\tilde{\omega}_{\rm ex}(\boldsymbol{q}_{\rm ex})=0$, bringing about a singular point in $\varepsilon^R(\boldsymbol{q},\omega)$ at $\omega=0$ and $\boldsymbol{q}=\boldsymbol{q}_{\rm ex}$ for $r_s > r_s^c$, a feature never seen in the conventional metals like the electron gas for $r_s < r_s^c$.

This paper is organized as follows: In Sec. II we derive the third sum rule for $n(\boldsymbol{p})$, with which we improve on the GZ scheme to calculate $n(\boldsymbol{p})$ in the electron gas. Our improved scheme works very well to obtain $n(\boldsymbol{p})$ up to $r_s \approx 22$. In Sec. III we calculate $S(\boldsymbol{q},\omega)$ with use of the obtained $n(\boldsymbol{p})$ and the local-field factor $G_s(\boldsymbol{q},\omega+i0^+)$, the latter of which is improved on the original form of Richardson and Ashcroft (RA). For r_s larger than about 10, a novel peak structure appears in $S(\boldsymbol{q},\omega)$ and it dominates the plasmon peak for $r_s > 20$. The origin of this peak is investigated by a detailed study of $\varepsilon^R(\boldsymbol{q},\omega)$. The results obtained in this paper are summarized in Sec. IV, together with discussions on related issues. In this paper, we employ units in which $\hbar = k_{\rm B} = 1$.

II. MOMENTUM DISTRIBUTION FUNCTION

A. Hamiltonian

Apart from a constant term, the first-principles Hamiltonian H for a system of N electrons interacting with each other through the Coulomb interaction in a periodic one-body potential is written in the plane-wave basis as[30]

$$H = H_0 + V + U, \tag{10}$$

with

$$H_0 = \sum_{\boldsymbol{p}\sigma} \varepsilon_{\boldsymbol{p}} c^+_{\boldsymbol{p}\sigma} c_{\boldsymbol{p}\sigma}, \tag{11}$$

$$V = \frac{1}{2}\sum_{\boldsymbol{q}\neq\boldsymbol{0}}\sum_{\boldsymbol{p}\sigma}\sum_{\boldsymbol{p}'\sigma'} V(\boldsymbol{q}) c^+_{\boldsymbol{p}+\boldsymbol{q}\sigma} c^+_{\boldsymbol{p}'-\boldsymbol{q}\sigma'} c_{\boldsymbol{p}'\sigma'} c_{\boldsymbol{p}\sigma}, \tag{12}$$

$$U = \sum_{\boldsymbol{p}\sigma}\sum_{\boldsymbol{G}\neq\boldsymbol{0}} U_{\boldsymbol{p},\boldsymbol{p}+\boldsymbol{G}} c^+_{\boldsymbol{p}\sigma} c_{\boldsymbol{p}+\boldsymbol{G}\sigma}, \tag{13}$$

where $c_{\boldsymbol{p}\sigma}$ is the annihilation operator of an electron with momentum $\boldsymbol{p}$ and spin σ and $\boldsymbol{G}$ is a reciprocal-lattice vector. If the electron density $n(=N/\Omega_t)$ is so low as to satisfy the condition of $p_{\rm F}a_0 \ll 1$, we may virtually regard $|\boldsymbol{G}|$, which is $2\pi/a_0$ or larger, as an infinite number, allowing us to neglect all terms in U. Then the system can be decribed by the Hamiltonian reduced in the form of $H = H_0 + V$, which is nothing but the electron gas and with which we shall be concerned in this paper.

B. Momentum distribution function

At zero temperature ($T=0$), the momentum distribution function $n(\boldsymbol{p})$ is defined as an expectation value

$$n(\boldsymbol{p}) = \langle c^+_{\boldsymbol{p}\sigma} c_{\boldsymbol{p}\sigma}\rangle, \tag{14}$$

evaluated with respect to the ground state Ψ_0. This quantity is independent of spin for a paramagnetic Ψ_0.

The short-range electron correlation determines the asymptotic behavior of $n(\boldsymbol{p})$ as well as the structure factor $S(\boldsymbol{q})$ and their exact forms are given as[31]

$$\begin{aligned}&\Omega_t \left(\frac{a_B}{4\pi}\right)^2 \lim_{|\boldsymbol{p}|\to\infty}\Big[|\boldsymbol{p}|^8 n(\boldsymbol{p})\Big] \\ &= \left(\frac{a_B}{8\pi}\right) \lim_{|\boldsymbol{q}|\to\infty}\Big[|\boldsymbol{q}|^4 S(\boldsymbol{q})\Big] = g(0),\end{aligned} \tag{15}$$

where $g(0)$ is the on-top value of the pair distribution function. We can rewite Eq. (15) as

$$\lim_{|\boldsymbol{p}|\to\infty} n(\boldsymbol{p}) = \frac{8}{9}\left(\frac{\alpha r_s}{\pi}\right)^2 \frac{p_{\rm F}^8}{|\boldsymbol{p}|^8}\, g(0), \tag{16}$$

dictating the asymptotic behavior of $n(\boldsymbol{p})$. By using $V(\boldsymbol{q})$ in the electron-electron ladder approximation, Yasuhara derived a formula for $g(0)$ as[32,33]

$$g(0) = g_{\rm Y}(0) \equiv \frac{1}{2}\left(\frac{\sqrt{4\alpha r_s/\pi}}{I_1(2\sqrt{4\alpha r_s/\pi})}\right)^2, \tag{17}$$

where $I_1(x)$ is the modified Bessel function of the first kind. There are three other parametrization formulas for $g(0)$; by the phase-shift analysis of the two-electron problem, Overhauser[34] devived one formula $g_{\rm O}(0)$ and Gori-Giorgi and Perdew[35] improved on it to give another one $g_{\rm GP}(0)$, both of which are intended to provide accurate results of $g(0)$ for $r_s \le 10$. More recently, Spink, Needs, and Drummond (SND)[6] provided yet another formula $g_{\rm SND}(0)$, which reproduces their DMC data for $r_s \le 20$. The results of those formulas are given as a function of r_s in Fig. 2. We see immediately that they are essentially the same for $r_s \le 10$. For $r_s \le 20$, Yasuhara's and SND's give about the same results, but the latter deteriorates very much soon after r_s goes beyond 20. (Actually, SND gives unphysical negative $g(0)$ for $r_s > 24.26$.) Thus, apparently, the best choice for $g(0)$ is the Yasuhara's formula $g_{\rm Y}(0)$ in Eq. (17) which will be mainly employed over a wide range of r_s hereafter.

C. Sum rules

Let us derive the three sum rules, Eqs. (3)-(5), for $n(\boldsymbol{p})$. The static charge response function $Q_c^R(\boldsymbol{q},0)$ in the electron gas is calculated by Moroni, Ceperley, and Senatore (MCS)[36] in DMC for $r_s \le 10$, giving the numerical data for $\Pi(\boldsymbol{q},0)$. With use of Eq. (8), we obtain

$$\frac{1}{\Pi(\boldsymbol{q},0)} = \frac{1}{\Pi_0(\boldsymbol{q},0)} - V(\boldsymbol{q}) G_+(\boldsymbol{q},0). \tag{18}$$

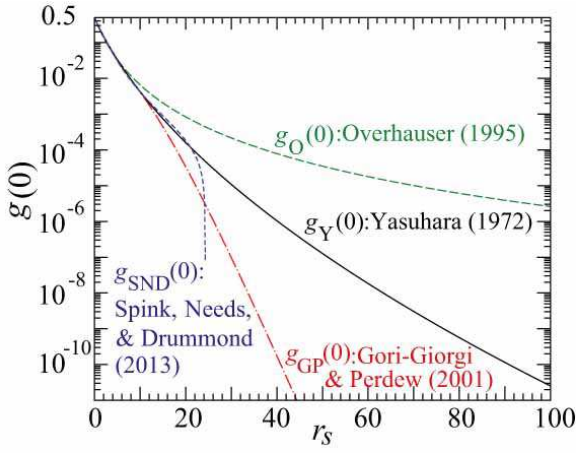

FIG. 2: (Color online) Comparison of various formulas for the on-top pair distribution function $g(0)$ plotted as a function of r_s over a very wide range.

This may be regarded as the definition of the static local-field factor $G_+(\boldsymbol{q},0)$. The DMC data of $\Pi(\boldsymbol{q},0)$, together with the well-known analytical result of $\Pi_0(\boldsymbol{q},0)$, determine $G_+(\boldsymbol{q},0)$, which is parametrized as a function of r_s and $q\,(=|\boldsymbol{q}|)$.[36] In particular, in the limit of $q\to\infty$, $G_+(\boldsymbol{q},0)$ is known as

$$G_+(\boldsymbol{q},0) \xrightarrow[q\to\infty]{} C(r_s)\left(\frac{q}{p_{\rm F}}\right)^2 + B(r_s), \tag{19}$$

where the constants $B(r_s)$ and $C(r_s)$ are given by

$$B(r_s) = B_{\rm MCS}(r_s) \equiv \frac{1+(a_1+a_2r_s)\sqrt{r_s}}{3+(b_1+b_2r_s)\sqrt{r_s}}, \tag{20}$$

$$C(r_s) = \frac{\pi}{4}\alpha r_s\left(-\varepsilon_c(r_s) - r_s\frac{\partial\varepsilon_c(r_s)}{\partial r_s}\right), \tag{21}$$

with $a_1 = 2.15$, $a_2 = 0.435$, $b_1 = 1.57$, $b_2 = 0.409$, and $\varepsilon_c(r_s)$ (in Ry) in the parameterization scheme due to Perdew and Wang.[4]

On the other hand, we obtain another expression for $\Pi(\boldsymbol{q},0)^{-1}$ with use of Eq. (6) as

$$\frac{1}{\Pi(\boldsymbol{q},0)} = \frac{1}{\Pi_{\rm WI}(\boldsymbol{q},0)} - V(\boldsymbol{q})G_s(\boldsymbol{q},0), \tag{22}$$

where the other local-field factor $G_s(\boldsymbol{q},0)$ was investigated by Niklasson[37] through the equation of motion method and is known to behave asymptotically as

$$G_s(\boldsymbol{q},0) \xrightarrow[q\to\infty]{} \frac{2}{3}\big[1-g(0)\big]. \tag{23}$$

By combining Eq. (22) with Eq. (18), we obtain

$$\frac{1}{\Pi_{\rm WI}(\boldsymbol{q},0)} = \frac{1}{\Pi_0(\boldsymbol{q},0)} + \big[G_s(\boldsymbol{q},0) - G_+(\boldsymbol{q},0)\big]\,V(\boldsymbol{q}). \tag{24}$$

Now $\Pi_{\rm WI}(\boldsymbol{q},0)$ in Eq. (7) is reduced to

$$\Pi_{\rm WI}(\boldsymbol{q},0) = \Omega_t\frac{mp_{\rm F}}{2\pi^2}\int_0^\infty dx\, n(x)\,\frac{x}{z}\,\ln\left|\frac{x+z}{x-z}\right|, \tag{25}$$

with $x = |\boldsymbol{p}|/p_{\rm F}$, $z = |\boldsymbol{q}|/2p_{\rm F}$, and $n(x) = n(\boldsymbol{p})$. This equation can be asymptotically expanded as

$$\Pi_{\rm WI}(\boldsymbol{q},0) = \Omega_t\frac{mp_{\rm F}}{\pi^2}\left(\frac{I_2}{z^2} + \frac{1}{3}\frac{I_4}{z^4} + \frac{1}{5}\frac{I_6}{z^6} + \cdots\right), \tag{26}$$

where the nth-power integral I_n is defined as

$$I_n = \int_0^\infty dx\, n(x)\, x^n. \tag{27}$$

A similar asymptotic expansion can be made for $\Pi_0(\boldsymbol{q},0)$ with I_n replaced by $I_n^{(0)} = 1/(n+1)$. Then, by comparing the both sides of Eq. (24) order by order and taking the large-q limit, we obtain the following set of equations:

$$I_2 = \frac{1}{3}, \tag{28}$$

$$I_4 = \frac{1}{5} + \frac{\alpha^2 r_s^2}{3}\left[-\varepsilon_c(r_s) - r_s\frac{\partial\varepsilon_c(r_s)}{\partial r_s}\right], \tag{29}$$

$$I_6 = \frac{8}{105} + \frac{5}{3}I_4^2 + \frac{5\alpha r_s}{9\pi}\left[B(r_s) - \frac{2}{3} + \frac{2}{3}g(0)\right]. \tag{30}$$

These equations correspond to Eqs. (3)-(5), respectively, and thus the sum rules are now proved. Note that with use of I_n and $E_{\rm F} = 1/(\alpha^2 r_s^2)$ (in Ry), we can write the average kinetic energy $\langle{\rm KE}\rangle$, the fluctuation of kinetic energy $\Delta{\rm KE}$, and $\Pi_{\rm WI}(\boldsymbol{0},0)$ as

$$\langle{\rm KE}\rangle \equiv \langle\varepsilon_{\boldsymbol{p}}\rangle = 3I_4\,E_{\rm F}, \tag{31}$$

$$\Delta{\rm KE} \equiv \sqrt{\langle(\varepsilon_{\boldsymbol{p}} - \langle\varepsilon_{\boldsymbol{p}}\rangle)^2\rangle} = \sqrt{3I_6 - 9I_4^2}\,E_{\rm F}, \tag{32}$$

$$\Pi_{\rm WI}(\boldsymbol{q},0) \xrightarrow[q\to0]{} \Pi_{\rm WI}(\boldsymbol{0},0) = \Omega_t\frac{mp_{\rm F}}{\pi^2}\,I_0. \tag{33}$$

D. Parametrization form of $n(\boldsymbol{p})$

Following Gori-Giorgi and Ziesche (GZ),[27] we consider $n(x)$ in the parametrization form of

$$n(x) = \begin{cases} n_0 - \dfrac{n_0-n_-}{G(0)}\,G(x_-) & \text{for } x<1, \\ \dfrac{n_+}{G(0)}\,G(x_+) & \text{for } x>1, \end{cases} \tag{34}$$

where x_- and x_+ are, respectively, introduced as

$$x_- = a_-(r_s)\frac{\alpha r_s}{2\pi^2}\frac{G(0)}{n_0-n_-}\frac{1-x}{\sqrt{4\alpha r_s/\pi}} + b(r_s)\frac{\pi^2}{\alpha r_s}\sqrt{\frac{\pi}{3}\frac{1-\ln 2}{F''(0)}\frac{n_0-n_-}{G(0)}}\,\frac{(1-x)^2}{x}, \tag{35}$$

with $F''(0)/2 = 8.984373$ and

$$x_+ = a_+(r_s)\frac{\alpha r_s}{2\pi^2}\frac{G(0)}{n_+}\frac{x-1}{\sqrt{4\alpha r_s/\pi}} + \sqrt{\frac{3\pi(1-\ln 2)}{g(0)}\frac{n_+}{G(0)}\frac{\pi}{4\alpha r_s}}\,(x-1)^4\,F_\infty(x). \quad (36)$$

Here $G(x)$ is the Kulik function,[38] defined as

$$G(x) = \int_0^\infty du \frac{R'(u)}{R(u)}\frac{u}{u+y}\frac{R(u)-R(y)}{u-y}\bigg|_{y=x/\sqrt{R(u)}}, \quad (37)$$

with $R(u) = 1 - u\arctan(1/u)$. This function appears in the calculation of $n(x)$ in the random-phase approximation (RPA) and its asymptotic behavior may be summarized as follows: in the small-x limit,

$$G(x \ll 1) = G(0) + \pi\left(\frac{\pi}{4} + \sqrt{3}\right) x\ln x + \cdots, \quad (38)$$

with

$$G(0) = \int_0^\infty du\,\frac{-R'(u)}{R(u)}\arctan\frac{1}{u} = 3.353337\cdots, \quad (39)$$

while in the large-x limit, we obtain

$$G(x \gg 1) = \frac{\pi}{6}(1-\ln 2)\frac{1}{x^2} + \cdots. \quad (40)$$

In accordance with this asymptotic behavior of $G(x)$, $n(x)$ in Eq. (34) behaves in the following way at various limits: In the limit of $x \to 0$,

$$n(x) \xrightarrow[x\to 0]{} n_0 - \frac{F''(0)}{2}\left(\frac{\pi}{\alpha}\right)^4\left(\frac{\alpha r_s}{b(r_s)}\right)^2 x^2. \quad (41)$$

By a simple interpolation between high- and low-density limits of the coefficient of the x^2 term in Eq. (41), GZ deduced $b(r_s)$ to be the form of

$$b(r_s) = (1 + 0.0009376925 r_s^{13/4})^{1/2}. \quad (42)$$

We adopt this form for $b(r_s)$. In the limit of $x \to 1$,

$$n(x) \xrightarrow[x\to 1+0^\pm]{} n_\pm \pm A_\pm(r_s)|1-x|\ln|1-x|, \quad (43)$$

with $A_\pm(r_s)$ "the Fermi-edge coefficient" or the coefficient of the logarithmic singularity of the derivative of $n(x)$ at $x = 1 \pm 0^+$, given by

$$A_\pm(r_s) = \frac{1}{4}\left(\frac{\pi}{4} + \sqrt{3}\right)\left(\frac{\alpha r_s}{\pi}\right)^{1/2} a_\pm(r_s) \approx 0.256\sqrt{r_s}\; a_\pm(r_s). \quad (44)$$

If the electron-hole symmetry strictly holds in the electronic excitations, we obtain $A_-(r_s) = A_+(r_s)$, as was assumed by GZ, but at low densities in which electron-hole excitations are not restricted only near the Fermi surface and/or the dispersion of a quasi-electron is different from that of a quasi-hole, the symmetry will be broken in general, requiring us to determine $A_-(r_s)$ and $A_+(r_s)$ separately. Finally in the limit of $x \gg 1$,

$$n(x) \xrightarrow[x\to\infty]{} \frac{8}{9}\left(\frac{\alpha r_s}{\pi}\right)^2\frac{1}{x^8}\frac{g(0)}{F_\infty(x)^2}. \quad (45)$$

If $F_\infty(x)$ approaches unity at $x \to \infty$, Eq. (45) is reduced to Eq. (16), as it should be. In fact, GZ took $F_\infty(x) \equiv 1$, but we can include the effect of the next-leading term of $O(x^{-10})$ at $x \gg 1$ by giving a form for $F_\infty(x)$ as

$$F_\infty(x) = \frac{(x-1)^2 + \exp[a_\infty(r_s)]}{(x-1)^2 + \exp[-a_\infty(r_s)]}, \quad (46)$$

where $a_\infty(r_s)$ is an adjustable parameter related to the coefficient of the next-leading term. Note that $F_\infty(x) \equiv 1$ for $a_\infty(r_s) \equiv 0$. In actual calculations, we find that $a_\infty(r_s)$ plays an important role in fulfulling the third sum rule, Eq. (30).

E. Input data for the parametrization scheme

There are six free parameters, namely, n_0, $n_\pm$, $a_\pm$, and a_∞, in the definition of Eq. (34). The basic idea of GZ is to determine the first three by the interpolation between the accurate data of $n(\boldsymbol{p})$ for $1 \le r_s \le 5$ obtained by EPX[9] and the result in the limit of $r_s \to \infty$ in which GZ assume that $n(\boldsymbol{p})$ is reduced to that in the Wigner lattice, $n_{\rm W}(\boldsymbol{p})$, expressed as

$$n_{\rm W}(\boldsymbol{p}) = \frac{4\pi}{3}\left(\frac{p_{\rm F}^2}{\pi m\omega}\right)^{3/2}\exp\left(-\frac{\boldsymbol{p}^2}{m\omega}\right), \quad (47)$$

with $\omega = 0.8833 r_s^{-3/2}$ in a.u. In improving on the GZ scheme, we also adopt $n_{\rm W}(\boldsymbol{p})$ as basic information for $r_s \gg 10$, but the EPX data are upgraded by the data for $1 \le r_s \le 10$ obtained by GWΓ (or actually G$\tilde{\rm W}\Gamma_{\rm WI}$).[10] Then the actual parameterization formulas for $n_0(r_s)$ and $n_\pm(r_s)$ are slightly different from those in GZ. Our revised results for them are given, respectively, by

$$n_0(r_s) = \frac{1 + t_1 r_s^2 + t_2 r_s^{5/2}}{1 + t_3 r_s^2 + t_4 r_s^{13/4}}, \quad (48)$$

$$n_-(r_s) = \frac{1 + v_1 r_s + v_2 r_s^{5/2}}{1 + v_3 r_s + v_4 r_s^2 + v_5 r_s^{13/4}}, \quad (49)$$

$$n_+(r_s) = \frac{q_1 r_s + q_2 r_s^{5/2}}{1 + q_3 r_s^{1/2} + q_4 r_s^{3/2} + q_5 r_s^{13/4}}. \quad (50)$$

with $t_1 = 0.013\,813\,294\,1$, $t_2 = 0.006\,504\,281\,94$, $t_3 = 0.025\,275\,492\,1$, $t_4 = 0.001\,015\,523\,77$, $v_1 = 0.198\,200\,080$, $v_2 = 0.001\,839\,431\,25$, $v_3 = 0.286\,719\,080$, $v_4 = 0.013\,899\,539\,9$, $v_5 = 0.000\,473\,501\,718$, $q_1 = 0.088\,519\,000$, $q_2 = 0.002\,142\,766\,78$, $q_3 = 0.387\,350\,521$, $q_4 = 0.079\,971\,845\,3$, and $q_5 = 0.000\,551\,585\,578$.

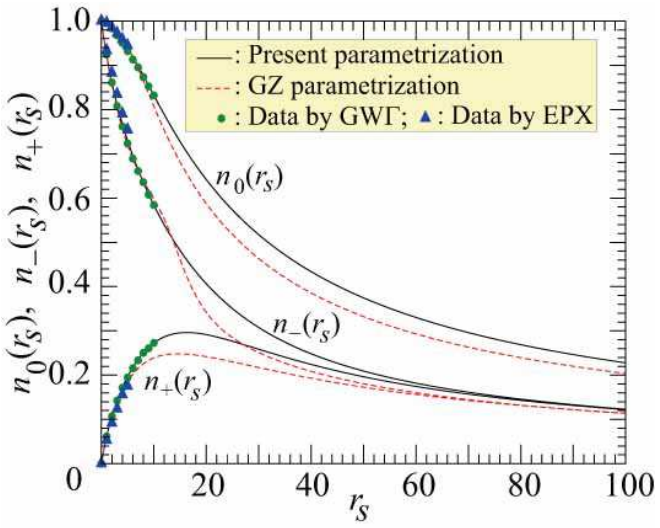

FIG. 3: (Color online) Parametrized n_0, n_-, and n_+ as a function of r_s in both present (solid curves) and Gori-Giorgi and Ziesche (dashed curves) schemes. The input data obtained by EPX (triangles) and GWΓ (solid circles) are also shown.

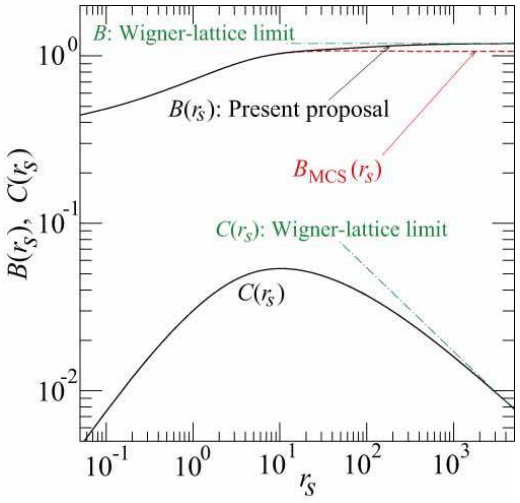

FIG. 4: (Color online) Parametrized $B(r_s)$ and $C(r_s)$ as a function of r_s. The former is compared with the one proposed by Moroni, Ceperley, and Senatore, together with the value in the Wigner-lattice limit.

The obtained $n_0(r_s)$ and $n_\pm(r_s)$ are plotted in Fig. 3. We see that our results are about the same as those in GZ for $r_s < 10$, but they are considerably different, especially for the case of $n_+(r_s)$; ours change much more smoothly with the increase of r_s than those in GZ and eliminate the strange behavior of $n_-(r_s)$ at $r_s \approx 16$ in GZ.

Incidentally, if we assume that $n(\boldsymbol{p})$ converges to $n_{\rm W}(\boldsymbol{p})$ in the low-density limit, we should assess this assumption by checking the three sum rules with this $n_{\rm W}(\boldsymbol{p})$ at $r_s \to \infty$. In fact, the first two sum rules are easily found to be satisfied, as already mentioned in GZ, but a problem exists on the third one; this $n_{\rm W}(\boldsymbol{p})$ gives $I_4 = 1/(2\varepsilon_{\rm W})$ and $I_6 = 5/(4\varepsilon_{\rm W}^2)$ with $\varepsilon_{\rm W} = p_{\rm F}^2/(m\omega) = 4.1692/\sqrt{r_s}$. By substituting those I_4 and I_6 into Eq. (30), we obtain $\lim_{r_s\to\infty} B(r_s) = 1.1868$, while $\lim_{r_s\to\infty} B_{\rm MCS}(r_s) = 1.064$, indicating the difference in about 10%. Because $B_{\rm MCS}(r_s)$ was determined with the input data only for $r_s \le 10$, we consider it more appropriate to amend $B(r_s)$ slightly from $B_{\rm MCS}(r_s)$ into a form fulfilling the asymptotic value of 1.1868 as

$$B(r_s) = \frac{1 + [a_1 + (a_2 + a_3 r_s) r_s]\sqrt{r_s}}{3 + [b_1 + (b_2 + b_3 r_s) r_s]\sqrt{r_s}}, \qquad (51)$$

with $a_1 = 2.161$, $a_2 = 0.4599$, $a_3 = 0.006679$, $b_1 = 1.594$, $b_2 = 0.4388$, and $b_3 = 0.005627$. In Fig. 4, this modified $B(r_s)$ is plotted in comparison with $B_{\rm MCS}(r_s)$ to find that they are essentially the same for $r_s \le 10$. The function $C(r_s)$ in Eq. (21) is also shown to see that $C(r_s)$ correctly behaves asymptotically in the Wigner-lattice limit.

F. Calculated results

The remaining three parameters, $a_\pm$ (or equivalently $A_\pm$) and a_∞, are determined so as to accurately satisfy the three sum rules at each r_s. The results for $n(\boldsymbol{p})$ calculated at $r_s = 8$ with use of three different forms, namely, Yasuhara, Overhauser, and GP, of $g(0)$ are shown in Fig. 5, together with those in the GZ scheme and GWΓ.[10] All these results are essentially the same, assuring that the present scheme works very well to obtain accurate enough $n(\boldsymbol{p})$ satisfying three sum rules simultaneously.

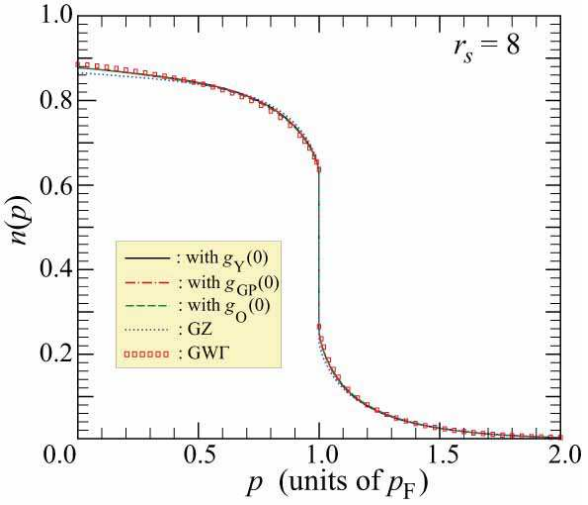

FIG. 5: (Color online) An example of $n(\boldsymbol{p})$ calculated with use of $g(0)$ in Yasuhara (solid), GP (dotted-dashed), and Overhauser (dashed) forms at $r_s = 8$. Our results are compared with that in the GZ scheme as well as that in GWΓ.

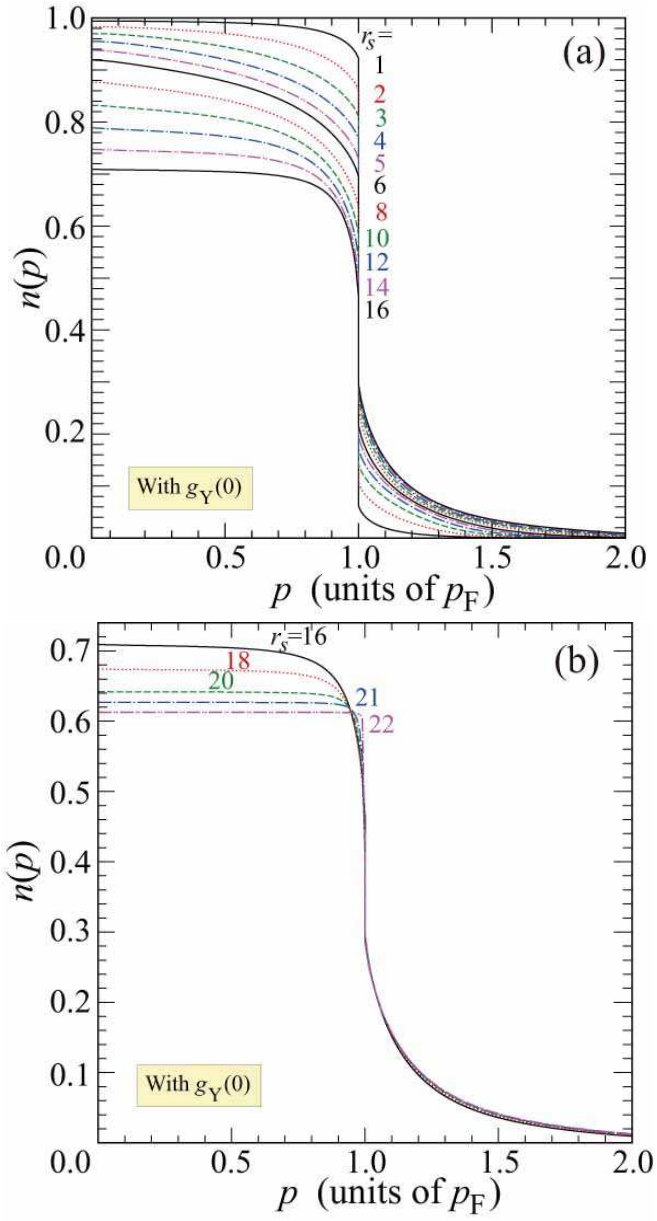

FIG. 6: (Color online) Obtained $n(\boldsymbol{p})$ for (a) $1 \le r_s \le 16$ and (b) $16 \le r_s \le 22$.

In Fig. 6, the results of $n(\boldsymbol{p})$ calculated with the choice of $g(0) = g_{\rm Y}(0)$ are shown for a wide range of r_s. In the metallic-density regime ($1 \le r_s \le 5$), the obtained $n(\boldsymbol{p})$ is about the same as that given in EPX[9] or GWΓ[22]. Even in the dielectric-catastrophe regime, $n(\boldsymbol{p})$ behaves in a normal and well-known manner, as long as r_s is smaller than about 12. With the further increase of r_s, however, it begins to behave rather differently from the normal one for $|\boldsymbol{p}| < p_{\rm F}$ and eventually for $r_s > 20$, it exhibits a novel feature in the sense that $n(\boldsymbol{p})$ becomes virtually flat for $|\boldsymbol{p}| < p_{\rm F}$, implying that the quasi-hole excitation energy at the center of the Fermi sphere is about the same as that near the Fermi surface. For $|\boldsymbol{p}| > p_{\rm F}$, on the other hand, this anomalous flat behavior is never seen in $n(\boldsymbol{p})$, indicating strong electron-hole asymmetric excitation spectra. Incidentally, a sign of this asymmetry has already been seen in the one-electron spectral function obtained in GWΓ at $r_s = 8$ (see, Fig. 3(b) in Ref. 10) and here we find that this tendency of asymmetry becomes so enhanced for $r_s > 20$ to provide the very characteristic flat behavior of $n(\boldsymbol{p})$ in Fig 6(b).

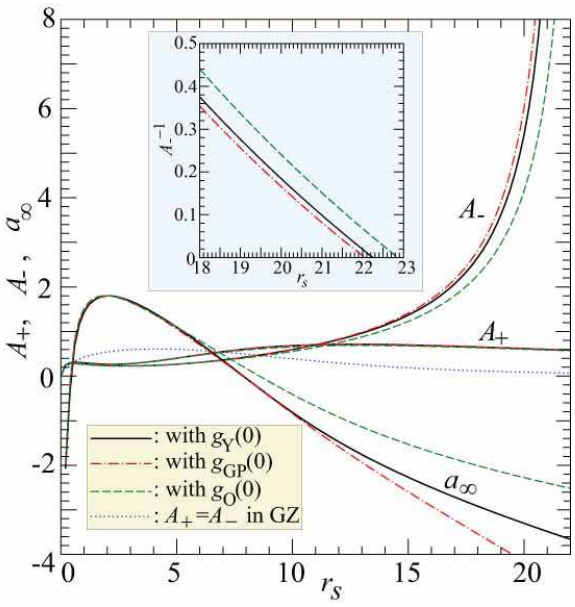

FIG. 7: (Color online) Parameters $A_\pm$ and a_∞ determined so as to satisfy the three sum rules for $n(\boldsymbol{p})$ at each r_s. Three different forms for $g(0)$ are employed. For comparison, $A_\pm$ in GZ are also shown. (In GZ, $a_\infty = 0$.) The inset displays A_-^{-1} for the region of r_s in which A_- is very large.

In Fig. 7, we plot the results for $A_\pm$ and a_∞ determined so as to satisfy the three sum rules, Eqs. (28)-(30), at each r_s. Three different forms for $g(0)$ are employed, but the obtained $A_\pm$ is virtually independent of its choice; the difference in $g(0)$ is mostly compensated by the difference in a_∞. The difference between A_+ and A_- indicates the degree of electron-hole asymmetry near the Fermi surface; for $r_s < 12$, they are essentially the same, but for $r_s \ge 12$, A_- rapidly increases, while A_+ does not change much. This asymmetry is probably the physical reason why the GZ scheme, in which $A_- = A_+$ was assumed, could not give a convergent result of $n(\boldsymbol{p})$ for $r_s > 12$.

In the parametrization scheme in Eq. (34), the behavior of $n(\boldsymbol{p})$ for $|\boldsymbol{p}| < p_{\rm F}$ is controlled only by the parameter A_- and thus its anomalous flat feature is directly connected with the rapid increase of A_- for $r_s > 12$. As shown in the inset of Fig. 7, A_- actually diverges at $r_s = \bar{r}_s^c = 22.4 \pm 0.4$, the error of which is deduced from the difference in $\bar{r}_s^c$ caused by the different choice of $g(0)$. For r_s beyond $\bar{r}_s^c$, our scheme does not work and fails to determine the three parameters, $A_\pm$ and a_∞, simultaneously satisfying three sum rules. We might be able to interpret this divergence of the Fermi-edge coeffi-

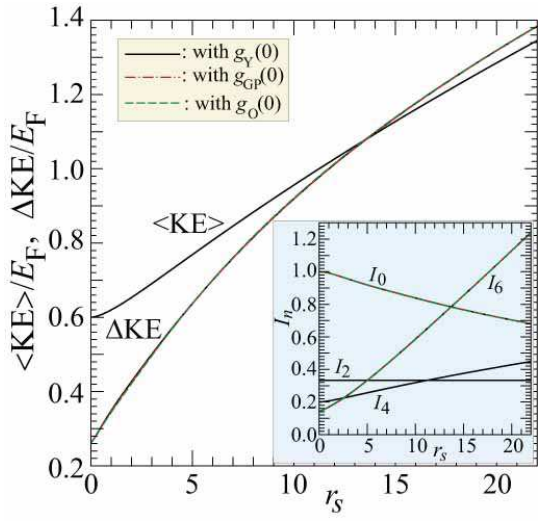

FIG. 8: (Color online) The average kinetic energy and the fluctuation of the kinetic energy as a function of r_s. No difference is seen by the different choice of $g(0)$ because of the fulfillment of the three sum rules. Inset: Corresponding values of I_n for $n = 0, 2, 4$, and 6.

cient or the nonanalytic behavior at the Fermi surface as an indication of the occurrence of some non-Fermi-liquid phase, but at present, we do not know exactly whether this is the case or not, mainly because we cannot rule out the possibility of inadequacy of the postulated form in Eq. (34) for the case of $A_- \gg 1$ (or $r_s > 20$). In any case, for $r_s \gtrsim 12$, it is certain that some unusual situation due to electron correlation begins to appear, as we can see in Fig. 8 in which the fluctuation of the kinetic energy ΔKE becomes larger than the average one $\langle$KE$\rangle$.

III. DYNAMICAL STRUCTURE FACTOR

A. Basic equation to determine $S(\boldsymbol{q},\omega)$

At $T = 0$, with use of Eq. (2) for $Q_c^R(\boldsymbol{q},\omega)$, $S(\boldsymbol{q},\omega)$ can be cast into the form of

$$S(\boldsymbol{q},\omega) = -\frac{1}{\pi}\frac{1}{V(\boldsymbol{q})}\mathrm{Im}\left[\frac{1}{\varepsilon^R(\boldsymbol{q},\omega)}\right], \tag{52}$$

with the retarded dielectric function $\varepsilon^R(\boldsymbol{q},\omega)$, given by

$$\begin{aligned}\varepsilon^R(\boldsymbol{q},\omega) &= 1 + V(\boldsymbol{q})\Pi^R(\boldsymbol{q},\omega) \\ &= 1 + V(\boldsymbol{q})\frac{\Pi^R_{\rm WI}(\boldsymbol{q},\omega)}{1 - G_s^R(\boldsymbol{q},\omega)V(\boldsymbol{q})\Pi^R_{\rm WI}(\boldsymbol{q},\omega)}.\end{aligned} \tag{53}$$

Here Eq. (6) is employed to write $\Pi^R(\boldsymbol{q},\omega)$ in terms of $\Pi^R_{\rm WI}(\boldsymbol{q},\omega)$ and $G_s^R(\boldsymbol{q},\omega)$, the latter of which is given by the analytic continuation of $G_s(\boldsymbol{q},i\omega)$ to the real axis in the complex upper ω-plane ($i\omega \to \omega + i0^+$). Thus our task to calculate $S(\boldsymbol{q},\omega)$ begins with obtaining both $\Pi^R_{\rm WI}(\boldsymbol{q},\omega)$ and $G_s^R(\boldsymbol{q},\omega)$.

B. Polarization function $\Pi^R_{\rm WI}(\boldsymbol{q},\omega)$

The function $\Pi_{\rm WI}(\boldsymbol{q},i\omega)$ in Eq. (7) is rewritten as

$$\begin{aligned}\Pi_{\rm WI}(\boldsymbol{q},i\omega) &= 2\sum_{\boldsymbol{p}\sigma} n(\boldsymbol{p})\frac{\varepsilon_{\boldsymbol{p}+\boldsymbol{q}} - \varepsilon_{\boldsymbol{p}}}{\omega^2 + (\varepsilon_{\boldsymbol{p}+\boldsymbol{q}} - \varepsilon_{\boldsymbol{p}})^2} \\ &= \Omega_t \frac{mp_{\rm F}}{2\pi^2} P_{\rm WI}(z, iu),\end{aligned} \tag{54}$$

with the function $P_{\rm WI}(z,iu)$, introduced as

$$P_{\rm WI}(z,iu) = \frac{1}{2z}\int_0^\infty x dx\, n(x) \ln\left[\frac{u^2 + (x+z)^2}{u^2 + (x-z)^2}\right], \tag{55}$$

where $x = |\boldsymbol{p}|/p_{\rm F}$, $z = |\boldsymbol{q}|/2p_{\rm F}$, and $u = (\omega/4E_{\rm F})/z$. By analytic continuation, $\Pi^R_{\rm WI}(\boldsymbol{q},\omega)$ is obtained as

$$\Pi^R_{\rm WI}(\boldsymbol{q},\omega) = \Omega_t \frac{mp_{\rm F}}{2\pi^2} P_{\rm WI}(z, u+i0^+), \tag{56}$$

with $P_{\rm WI}(z,u+i0^+)$, given by

$$\begin{aligned}P_{\rm WI}(z,u+i0^+) = \frac{1}{2z}\int_0^\infty x dx\, n(x)\Big\{&\ln[u^2 - (x+z)^2 + i0^+] \\ &- \ln[u^2 - (x-z)^2 + i0^+]\Big\},\end{aligned} \tag{57}$$

where $\ln(\omega)$ is so defined as $\ln(\omega) = \ln(|\omega|) + i\arg(\omega)$ with $\arg(\omega)$ the argument of ω in the upper ω-plane being between 0 and π. In performing the numerical evaluation of this integral over the variable x, care must be exerted at both $x = |u - z|$ and $x = u + z$ in order to accurately obtain the principal values of the integral.

With $n(\boldsymbol{p})[= n(x)]$ obtained in Sec. II F, we can calculate $\Pi^R_{\rm WI}(\boldsymbol{q},\omega)$ through Eqs. (56) and (57). The overall structure of the calculated $\Pi^R_{\rm WI}(\boldsymbol{q},\omega)$ does not depend much on r_s, in spite of the apperance of an anomalous feature in $n(\boldsymbol{p})$ for $r_s > 20$; as shown in Fig. 9, even at $r_s = 22$, the results of $\Pi^R_{\rm WI}(\boldsymbol{q},\omega)$ given as a function of ω at various values of $\boldsymbol{q}$ (the solid curves) retain the main features of those of $\Pi_0^R(\boldsymbol{q},\omega)$ the Lindhard function in the retarded form (the dotted-dashed curves). We can understand this insensitivity of $\Pi^R_{\rm WI}(\boldsymbol{q},\omega)$ to the anomalous feature in $n(\boldsymbol{p})$ by paying attention to the fact that $\Pi^R_{\rm WI}(\boldsymbol{q},\omega)$ is mostly controlled by the sum rules for $n(\boldsymbol{p})$; the details of $n(\boldsymbol{p})$ are smeared out by the integral over the variable x in Eq. (57).

Note, however, that there is a very important difference between $\Pi_0^R(\boldsymbol{q},\omega)$ and $\Pi^R_{\rm WI}(\boldsymbol{q},\omega)$; $\mathrm{Im}\Pi_0^R(\boldsymbol{q},\omega)$ does not vanish only in the electron-hole single-pair excitation region in $(\boldsymbol{q},\omega)$ space, while basically $\mathrm{Im}\Pi^R_{\rm WI}(\boldsymbol{q},\omega)$ is not zero but positive definite for $\omega > 0$ at any $\boldsymbol{q}$ due to the inclusion of the multiple electron-hole pair excitations by the use of $n(\boldsymbol{p})$ instead of $n_0(\boldsymbol{p})$. For this reason, as long as Eq. (53) is employed, we do not need to introduce an artificial finite broadening width γ in the numerical calculation of the dielectric function, in sharp contrast with the usual treatment of $\omega \to \omega + i\gamma$ in the calculation of the plasmon-peak structure in $S(\boldsymbol{q},\omega)$ with using $\Pi_0^R(\boldsymbol{q},\omega)$ or its simple extension in which no account is taken of the multiple electron-hole pair excitations.

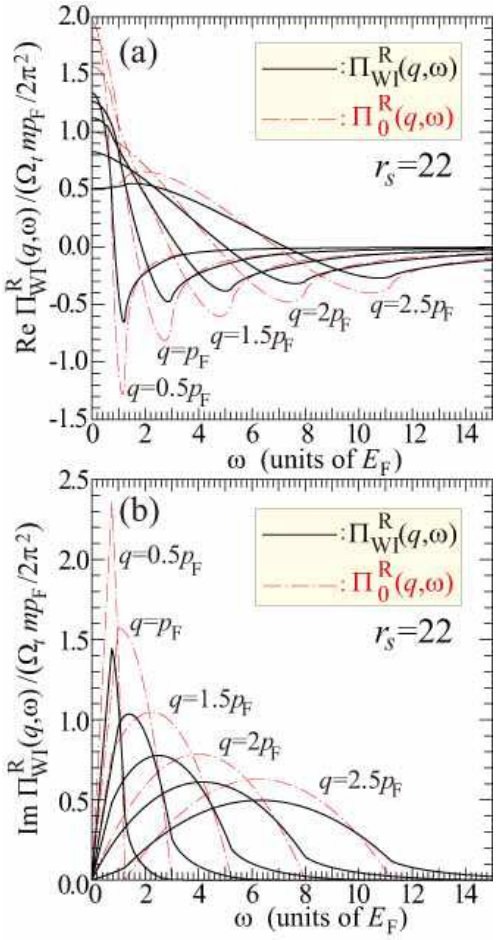

FIG. 9: (Color online) The retarded polarization function $\Pi^R_{\rm WI}(\boldsymbol{q},\omega)$ in comparison with $\Pi^R_0(\boldsymbol{q},\omega)$ at $r_s = 22$ for (a) real and (b) imaginary parts.

C. Dynamical local-field factor $G^R_s(\boldsymbol{q},\omega)$

There is a long history of researches on the dynamical local-field factor and its parametrization.[29,39–46] Those studies are mainly motivated by the construction of the exchange-correlation kernel $f_{\rm xc}(\boldsymbol{r},\boldsymbol{r}';\omega)$ in the time-dependent density functional theory (TDDFT) and thus they are concerned with either $G_+(\boldsymbol{q},i\omega)$ or $G^R_+(\boldsymbol{q},\omega)$, but not with $G_s(\boldsymbol{q},i\omega)$. So far a parametrization form for $G_s(\boldsymbol{q},i\omega)$ is given only by RA[28], proposing

$$G_s(\boldsymbol{q},i\omega) = \frac{a_s(i\Omega)z^2 + 2[1-g(0)]b_s(i\Omega)z^8/3}{1 + c_s(i\Omega)z^2 + b_s(i\Omega)z^8}, \qquad (58)$$

with $\Omega \equiv zu = \omega/4E_{\rm F}$. This form of $G_s(\boldsymbol{q},i\omega)$ satisfies the rigorous limit due to Niklasson[37] at $|\boldsymbol{q}| \to \infty$ as $G_s(\boldsymbol{q},i\omega) \to 2[1-g(0)]/3$, irrespective of ω.

The function $a_s(i\Omega)$ is so determined as to satisfy the constraints in the small-$|\boldsymbol{q}|$ regime, namely, the compressibility sum rule at $\Omega = 0$ and the third-moment sum rule[47–49] at $\Omega \to \infty$, leading to the following form:

$$a_s(i\Omega) = \lambda_s^{(\infty)} + \frac{\lambda_s^{(0)} - \lambda_s^{(\infty)}}{1 + \beta_1\gamma_s\Omega + (\beta_2\gamma_s\Omega)^2}, \qquad (59)$$

where $\lambda_s^{(0)}$ and $\lambda_s^{(\infty)}$ are, respectively, defined as

$$\lambda_s^{(0)} = \frac{\pi}{\alpha r_s}\left(\frac{1}{I_0} - \frac{\kappa_F}{\kappa}\right), \qquad (60)$$

$$\lambda_s^{(\infty)} = \frac{3}{5} - \frac{2}{5}\pi\alpha r_s\left[r_s\frac{\partial\varepsilon_c(r_s)}{\partial r_s} + 2\varepsilon_c(r_s)\right], \qquad (61)$$

where the ratio of the compressibilities with and without the interactions, κ and κ_F, can be calculated as

$$\frac{\kappa_F}{\kappa} = 1 - \frac{\alpha r_s}{\pi} + \frac{\alpha^2 r_s^3}{6}\left[r_s\frac{\partial^2\varepsilon_c(r_s)}{\partial r_s^2} - 2\frac{\partial\varepsilon_c(r_s)}{\partial r_s}\right]. \qquad (62)$$

As for the two functions, $c_s(i\Omega)$ and $b_s(i\Omega)$, in Eq. (58), by the consideration of the condition to obtain the maximum value of $4[1-g(0)]/3$ for $G_s(\boldsymbol{q},i\omega)$ at $z^2 \approx \Omega \to \infty$, RA gave the following forms:

$$c_s(i\Omega) = \frac{3}{4}\frac{\lambda_s^{(\infty)}}{1-g(0)} - \frac{\frac{4}{3} - \frac{1}{\alpha_{\rm RA}} + \frac{3}{4}\frac{\lambda_s^{(\infty)}}{1-g(0)}}{1+\gamma_s\Omega}, \qquad (63)$$

$$b_s(i\Omega) = \frac{a_s(i\Omega)}{3a_s(i\Omega) - 2[1-g(0)][3c_s(i\Omega) + 4/(1+\Omega)]/3} \times \frac{1}{1 + \gamma_1\Omega + \gamma_2\Omega^2 + \gamma_3\Omega^3 + \Omega^4}, \qquad (64)$$

with the parameter γ_s determined as

$$\gamma_s = \frac{9}{16}\frac{\lambda_s^{(\infty)}}{1-g(0)} + 1 - \frac{3}{4}\frac{1}{\alpha_{\rm RA}}. \qquad (65)$$

In Eqs. (59), (63), and (64), six parameters, $\alpha_{\rm RA}$, β_1, β_2, γ_1, γ_2, and γ_3, are at our disposal, but RA made the following choice: $\alpha_{\rm RA} = 0.9$, $\beta_1 = 0$, $\beta_2 = 1$, $\gamma_1 = \gamma_3 = 4$, and $\gamma_2 = 6$.

A similar parametrization scheme was proposed by RA for $G_n(\boldsymbol{q},i\omega)[\equiv G_+(\boldsymbol{q},i\omega) - G_s(\boldsymbol{q},i\omega)]$. As a matter of fact, with use of Eq. (24), $G_n(\boldsymbol{q},i\omega)$ is given exactly as

$$G_n(\boldsymbol{q},i\omega) = G_n^{\rm exact}(\boldsymbol{q},i\omega) \equiv \frac{1}{V(\boldsymbol{q})}\left[\frac{1}{\Pi_0(\boldsymbol{q},i\omega)} - \frac{1}{\Pi_{\rm WI}(\boldsymbol{q},i\omega)}\right]. \qquad (66)$$

We have calculated $G_n^{\rm exact}(\boldsymbol{q},i\omega)$ through Eq. (66) with $\Pi_{\rm WI}(\boldsymbol{q},i\omega)$ given by Eqs. (54) and (55) and compared with $G_n^{\rm RA}(\boldsymbol{q},i\omega)$, the parametrized form for $G_n(\boldsymbol{q},i\omega)$ due to RA, to find that $G_n^{\rm RA}(\boldsymbol{q},i\omega)$ is in fact very reliable; in particular, no appreciable difference can be seen for the quantities given by integrals over $\boldsymbol{q}$ and ω, such as $\varepsilon_c(r_s)$ obtained through the adiabatic connection formula, Eq. (27) in Ref. 29, in which we have calculated with use of either $G_s(\boldsymbol{q},i\omega) + G_n^{\rm RA}(\boldsymbol{q},i\omega)$ or

$G_s(\boldsymbol{q},i\omega)+G_n^{\rm exact}(\boldsymbol{q},i\omega)$. With this assessment of the RA parametrization scheme, we can expect that the parametrized $G_s(\boldsymbol{q},i\omega)$ will also be reliable. Incidentally, this RA scheme comes to be known to possess a very good feature[29]; it provides a quite accurate $\varepsilon_c(r_s)$ in reference to its "exact" value $\varepsilon_c^{\rm exact}(r_s)$ given by Perdew and Wang[4] (see the dotted-dashed curve in Fig. 10).

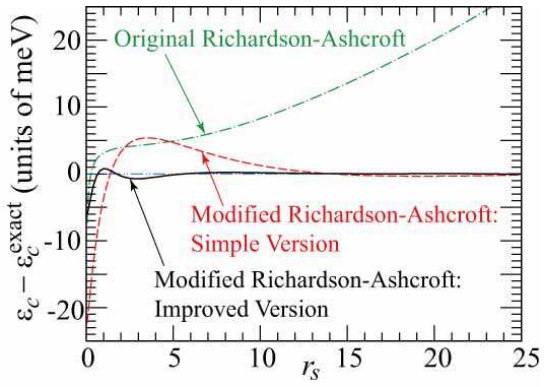

FIG. 10: (Color online) Difference between the "exact" value of ε_c due to Perdew and Wang and the one calculated through the adiabatic connection formula with using the local-field factor in the original RA (the dotted-dashed curve), a simple version of the modified RA (the dashed curve), and an improved version of the modified RA (the solid curve) schemes.

By analytic continuation ($i\omega\to\omega+i0^+$), we obtain $G_s^R(\boldsymbol{q},\omega)$ from $G_s(\boldsymbol{q},i\omega)$ in Eq. (58), but with β_is chosen in RA, $G_s^R(\boldsymbol{q},\omega)$ at small $\boldsymbol{q}$ suffers from the existence of unphysical divergence at $\omega=\pm 4E_{\rm F}/\gamma_s$. A simple way to eliminate this unphysical divergence while keeping the good feature of providing accurate $\varepsilon_c(r_s)$ is found to choose $\alpha_{\rm RA}=0.958/(1+0.006r_s)$, $\beta_1=0.8$, and $\beta_2=0.4$ with γ_is unchanged. This simple version of the modified RA scheme gives better $\varepsilon_c(r_s)$ than the original RA scheme (see Fig. 10). A closer analysis of this scheme, however, reveals that unphysical divergence appears for $2p_{\rm F}\lesssim|\boldsymbol{q}|\lesssim 3p_{\rm F}$ with γ_is chosen as those in RA.

Under these circumstances, we have made an extensive search of suitable values for all free parameters in Eqs. (59), (63), and (64) with considering the following four criteria; (i) $G_s^R(\boldsymbol{q},\omega)$ contains no unphysical divergence for real ω, (ii) $G_s^R(\boldsymbol{q},\omega)$ should be analytic in the upper complex ω-plane, in accord with the causality condition,[39,40] (iii) $G_s(\boldsymbol{q},i\omega)$ accurately provides ε_c in a wide range of r_s, and (iv) $G_s^R(\boldsymbol{q},\omega)$ combined with $\Pi_{\rm WI}^R(\boldsymbol{q},\omega)$ gives the results of $S(\boldsymbol{q},\omega)$ in good agreement with those in GWΓ[25] for $1\le r_s\le 5$. As a result of this search, we have chosen the following set of parameters, which we call an improved version of the modified RA scheme; $\beta_1=\beta_2=0.8$, $\gamma_1=\gamma_2=\gamma_3=1$ and

$$\alpha_{\rm RA}(r_s)=\frac{\alpha_0}{1+[\alpha_1+\alpha_2/(1+\alpha_3 r_s+\alpha_4 r_s^2)]\,r_s}, \qquad (67)$$

with $\alpha_0=1.2110$, $\alpha_1=0.01064$, $\alpha_2=0.10296$, $\alpha_3=-0.2910$, and $\alpha_4=0.2540$.

D. Ghost exciton mode $\tilde{\omega}_{\rm ex}(\boldsymbol{q})$

With $\Pi_{\rm WI}(\boldsymbol{q},i\omega)$ and $G_s(\boldsymbol{q},i\omega)$ thus determined, we can calculate $\Pi(\boldsymbol{q},i\omega)$ through Eq. (6) to find that it actually diverges at $i\omega=\pm i\tilde{\omega}_{\rm ex}(\boldsymbol{q})$ for $r_s>r_s^c$ in accord with the discussion in Ref. 21. Numerically, $\tilde{\omega}_{\rm ex}(\boldsymbol{q})$ can be determined by the search of zero of $\Pi(\boldsymbol{q},i\omega)^{-1}$ for $\omega>0$.

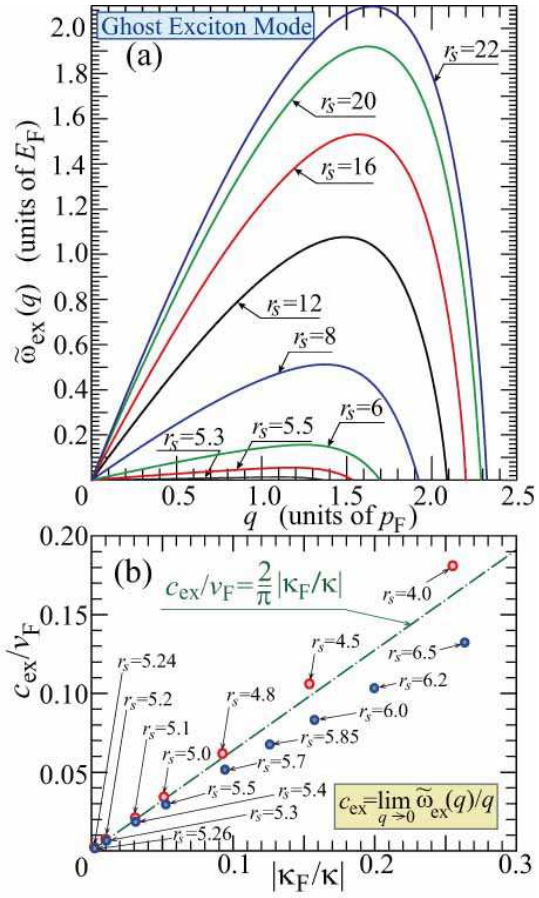

FIG. 11: (Color online) (a) Dispersion relation of the ghost exciton mode at various values of r_s.(b) Sound velocity of the ghost exciton mode in units of the Fermi velocity $v_{\rm F}$ plotted as a function of $|\kappa_F/\kappa|$.

In Fig. 11(a), the obtained results of $\tilde{\omega}_{\rm ex}(\boldsymbol{q})$ are shown as a function of $q(=|\boldsymbol{q}|)$ at several values of r_s in the dielectric-catastrophe regime of $r_s>r_s^c$. For small q, $\tilde{\omega}_{\rm ex}(\boldsymbol{q})$ increases in proportion to q, just like a sound mode, and "the sound velocity" $c_{\rm ex}$ changes in proportion to $|\kappa_F/\kappa|$ with the coefficient $2v_{\rm F}/\pi$ ($v_{\rm F}$: the Fermi velocity) for r_s near r_s^c, as shown in Fig. 11(b). Note that this behavior of $c_{\rm ex}$ is quite similar to that for "the exciton mode" identified by the peak position of ${\rm Im}\,\varepsilon^R(\boldsymbol{q},\omega)$ for $r_s<r_s^c$.[20] Thus it is more appropriate to call the mode of $\tilde{\omega}_{\rm ex}(\boldsymbol{q})$ on the imaginary ω axis "the ghost exciton mode" than "the ghost plasmon" which was suggested in Ref. 21.

The oscillator strength $f_{\rm ex}(\boldsymbol{q})$ in the definition of $\Pi_a(\boldsymbol{q},i\omega)$ in Eq. (1) is determined by the evaluation of

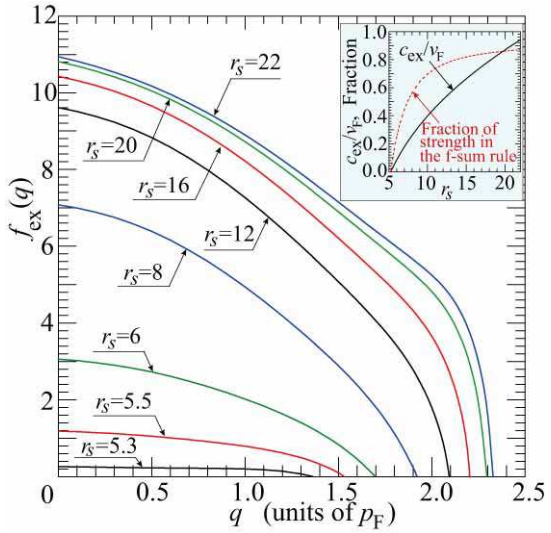

FIG. 12: (Color online) Oscillator strength of the ghost exciton mode. Inset: Fraction of this oscillator strength to the full strengths in the limit of $q \to 0$, together with the sound velocity in units of v_F, plotted as a function of r_s.

$[\omega - \tilde{\omega}_{ex}(\boldsymbol{q})]\Pi(\boldsymbol{q}, i\omega)$ in the limit of $\omega \to \tilde{\omega}_{ex}(\boldsymbol{q})$ and the obtained results are shown in Fig. 12. Incidentally, the asymptotic behavior of $\Pi(\boldsymbol{q}, i\omega)$ in Eq. (6) is found to be

$$\Pi(\boldsymbol{q}, i\omega) \xrightarrow[\omega\to\infty]{} \frac{4\pi}{V(\boldsymbol{q})} \frac{ne^2}{m} \frac{1}{\omega^2}, \tag{68}$$

from which we can prove the f-sum rule for $S(\boldsymbol{q}, \omega)$ as

$$\int_{-\infty}^{\infty} d\omega\, \omega S(\boldsymbol{q}, \omega) = \frac{N\boldsymbol{q}^2}{2m}. \tag{69}$$

On the other hand, $\Pi_a(\boldsymbol{q}, i\omega)$ behaves as

$$\Pi_a(\boldsymbol{q}, i\omega) \xrightarrow[\omega\to\infty]{} \frac{1}{V(\boldsymbol{q})} \frac{ne^2}{m} \frac{f_{ex}(\boldsymbol{q})}{\omega^2}. \tag{70}$$

Comparison of Eq. (70) with Eq. (68) indicates that the ghost exciton mode contributes to the full oscillator strengths with the fraction of $f_{ex}(\boldsymbol{q})/4\pi$, which becomes more than 80% at $q \to 0$ for $r_s > 14$. Thus, in such a dilute electron gas, we come to notice that not the plasmon but the exciton mode will play a main role in the whole excitation spectra.

E. Calculated results of $S(\boldsymbol{q}, \omega)$

With $\Pi^R_{WI}(\boldsymbol{q}, \omega)$ and $G^R_s(\boldsymbol{q}, \omega)$ already given, we can calculate $S(\boldsymbol{q}, \omega)$ through Eqs. (52) and (53). As mentioned before, in the usual metallic region ($1 \le r_s \le 5$), the form of $G^R_s(\boldsymbol{q}, \omega)$ is finely tuned to reproduce the results of $S(\boldsymbol{q}, \omega)$ that are already obtained in Ref. 25. As illustrated in Fig. 1(a) for $r_s = 4$, the structure of $S(\boldsymbol{q}, \omega)$

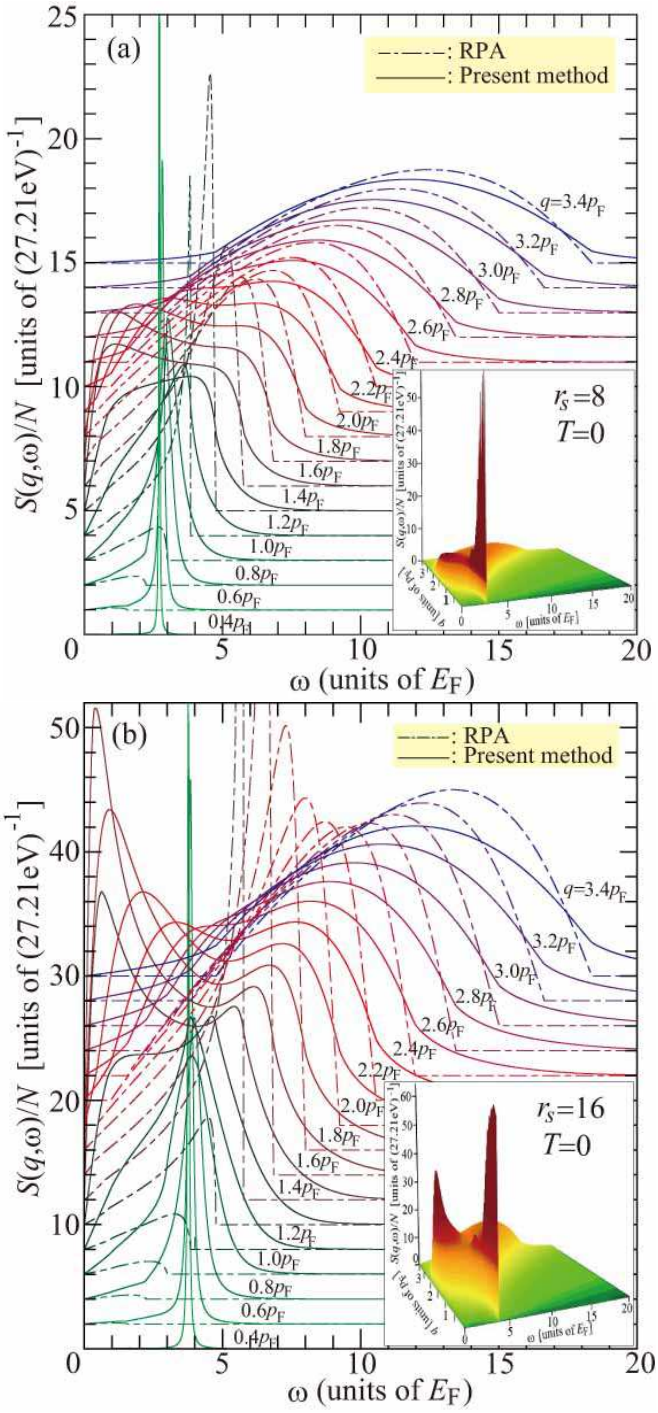

FIG. 13: (Color online) The Dynamical structure factor at (a) $r_s = 8$ and (b) $r_s = 16$. Inset: Bird's-eye view.

is featured by the single plasmon peak and the exciton contribution appears not as a peak but only as a shoulder structure in the low-ω region. (To be more definite, see the structure "a" specified in Fig. 1 in Ref. 25.)

Even in the dielectric-catastrophe regime ($r_s > r_s^c$), the main feature of $S(\boldsymbol{q}, \omega)$ hardly changes at r_s near r_s^c,

but as r_s increases further, the shoulder structure due to the excitonic effect gradually evolves into a broad peak, as illustrated in Fig. 13(a) at $r_s = 8$. The peak becomes sharper with the further increase of r_s and appears as a clear peak for $r_s \approx 10$. Eventually for $r_s \gtrsim 14$, combined with the plasmon peak, $S(\boldsymbol{q}, \omega)$ is characterized by a twin-peak structure, as shown at $r_s = 16$ in Fig. 13(b). At $r_s = 20$ or larger, "the excitonic peak" grows even bigger than the plasmon one [see Fig. 1(b)].

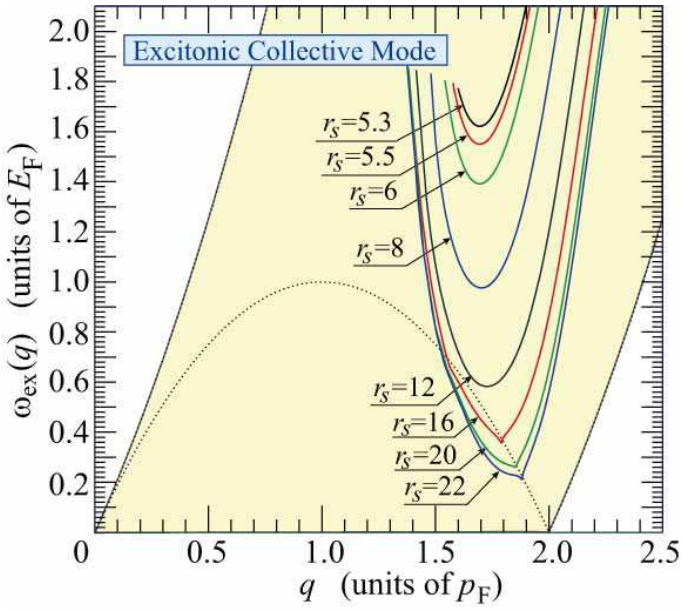

FIG. 14: (Color online) Dispersion relation of the excitonic collective mode as determined from the peak position in $S(\boldsymbol{q}, \omega)$ in (q, ω) space. The shaded area represents the electron-hole single-pair excitation region and the dotted curve indicates the boundary of $\omega = (2p_F q - q^2)/2m$.

In Fig. 14, we have plotted $\omega_{ex}(q)$ the excitonic peak position (including the shoulder position, if a peak structure is not well identified) at each q in (q, ω) space. This plot shows that $\omega_{ex}(q)$ is always inside the single-pair excitation region, as it should be for the excitonic effect working on an electron-hole single-pair excitation.

An even more interesting fact is that if $\omega_{ex}(q)$ is in the region of $\omega \leq (2p_F q - q^2)/2m$, the corresponding peak in $S(\boldsymbol{q}, \omega)$ is very sharp. In particular, $\omega_{ex}(q)$ becomes lowest if it lies just on this boundary and the highest peak in $S(\boldsymbol{q}, \omega)$ appears in its very vicinity. Furthermore, with the increase of r_s, this lowest-energy peak position $(q_{min}, \omega_{ex}(q_{min}))$ becomes lower approximately in proportion to r_s along the boundary curve, so that with the further increase of r_s up to about 30, we may imagin a critical situation of $q_{min} \to 2p_F$ and $\omega_{ex}(q_{min}) \to 0$ by extrapolation. If this critical situation were actually realized, we might expect the occurrence of a very exotic phase transition brought about by the spontaneous excitation of a macroscopic number of excitons or "the exciton condensation".

F. Retarded dielectric function $\varepsilon^R(\boldsymbol{q}, \omega)$

Let us make a detailed analysis of the retarded dielectric function $\varepsilon^R(\boldsymbol{q}, \omega)$ in order to investigate the relation between the excitonic-peak position (or the excitonic collective mode) $\omega_{ex}(q)$ and the ghost exciton mode $\tilde{\omega}_{ex}(\boldsymbol{q})$.

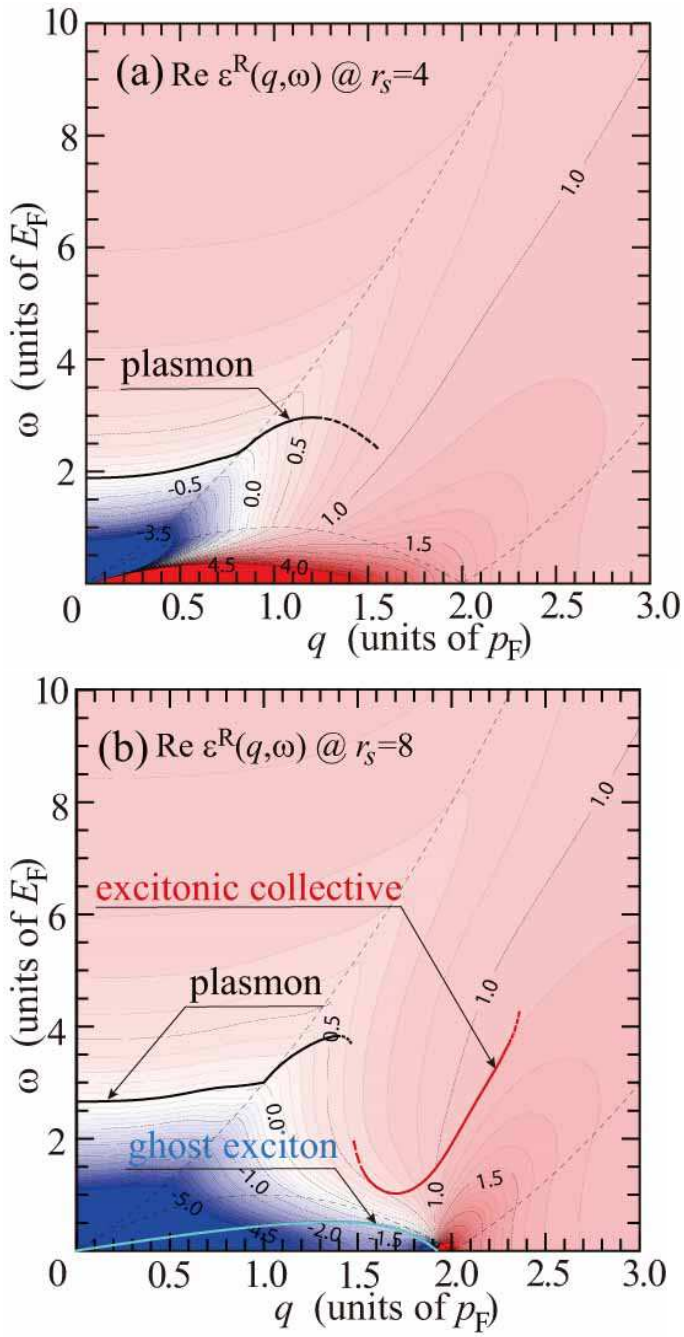

FIG. 15: (Color online) Two-dimensional contour map of the real part of $\varepsilon^R(\boldsymbol{q}, \omega)$ at (a) $r_s = 4$ and (b) $r_s = 8$.

In the conventional metals without the dielectric catastrophe as represented by the electron gas at $r_s = 4$, the

overall behavior of $\varepsilon^R(\boldsymbol{q},\omega)$ is well known and rather simple; as shown in Fig. 15(a) for its real part in (q,ω) space, there is only a single singular point at $q=\omega=0$ in this function, characterized by $\varepsilon^R(\boldsymbol{q},\omega)\approx 1-\omega_{pl}^2/\omega^2$ in the limit of $\omega\to 0$ with keeping $v_{\rm F}q/\omega\ll 1$ (the ω-limit) and $\varepsilon^R(\boldsymbol{q},\omega)\approx 1+(\kappa/\kappa_F)q_{\rm TF}^2/q^2$ in the limit of $q\to 0$ with $v_{\rm F}q/\omega\gg 1$ (the q-limit), where $\omega_{pl}(=\sqrt{4\pi e^2 n/m})$ is the plasmon energy at $q\to 0$ and $q_{\rm TF}(=\sqrt{4e^2 m p_{\rm F}/\pi})$ is the Thomas-Fermi screening constant. Associated with this singular point at the origin of (q,ω) space, the plasmon emerges as a collective mode satisfying $\varepsilon^R(\boldsymbol{q},\omega)\approx 0$ at $\omega\approx\omega_{pl}$ for small q.

In the dielectric-catastrophe regime ($r_s>r_s^c$), there appears the ghost exciton mode, but as long as $\tilde{\omega}_{\rm ex}(\boldsymbol{q})$ is positive, the mode is not a pole on the real axis in the complex ω-plane, indicating its irrelevance from a physical point of view. At both $q=0$ and $q_{\rm ex}(\neq 0)$ at which $\tilde{\omega}_{\rm ex}(\boldsymbol{q})$ becomes zero [see Fig. 11(a)], however, the pole is situated on the real axis and thus it must have direct physical relevance.

In fact, we find that $\varepsilon^R(\boldsymbol{q},\omega)$ contains a couple of singularities, one at the origin of (q,ω) space and the other at $q=q_{\rm ex}$ and $\omega=0$, as illustrated in Fig. 15(b) for the case of $r_s=8$. The singularity occurring at the origin behaves in much the same way as that in the conventional metals, excluding a possibility of the observation of any exotic effects associated with this singularity. The only difference in the case of negative κ from that of the conventional metals is seen in the sign of ${\rm Re}\,\varepsilon^R(\boldsymbol{q},\omega)$ in the q-limit and concomitantly the reduction of the oscillator strength for the plasmon pole, but this reduction never becomes perfect (see Fig. 12), allowing the existence of the plasmon at any value of r_s.

The singularity at $q=q_{\rm ex}$ and $\omega=0$, on the other hand, has not been discussed in the literature and thus a detailed analysis is needed here. In the vicinity of this singularity, $\varepsilon^R(\boldsymbol{q},\omega)$ is expressed as

$$\varepsilon^R(\boldsymbol{q},\omega)\approx 1+\left(\frac{p_{\rm F}}{q}\right)^2\frac{1}{A_{\rm ex}(q-q_{\rm ex})/p_{\rm F}-iB_{\rm ex}\omega/E_{\rm F}},\quad(71)$$

where the coefficients, $A_{\rm ex}$ and $B_{\rm ex}$, are given by $A_{\rm ex}=p_{\rm F}\partial f(q_{\rm ex},0)/\partial q_{\rm ex}$ and $B_{\rm ex}=-\lim_{\omega\to 0}E_{\rm F}{\rm Im}f(q_{\rm ex},\omega)/\omega$ with $f(q,\omega)$, defined in reference to Eq. (53) by

$$f(q,\omega)=\frac{\pi}{2}\frac{1}{\alpha r_s}\frac{1}{P_{\rm WI}(q,\omega)}-\left(\frac{p_{\rm F}}{q}\right)^2 G_s^R(q,\omega).\quad(72)$$

Note that $f(q_{\rm ex},0)=0$ by the definition of $q_{\rm ex}$.

In Fig. 16(a), the obtained $q_{\rm ex}$, $A_{\rm ex}$, and $B_{\rm ex}$ are plotted as a function of r_s. At $r_s=r_s^c$, $A_{\rm ex}$ vanishes, removing this singularity from $\varepsilon^R(\boldsymbol{q},\omega)$, but $A_{\rm ex}$ is positive definite for $r_s>r_s^c$ and thus this singularity always exists in the dielectric-catastrophe regime. With the increase of r_s, $q_{\rm ex}$ increases monotonically and at $r_s\approx 9.51$ it becomes equal to $2p_{\rm F}$, which is the boundary at the electron-hole single-pair excitation. Due to this transition across the boundary, both $A_{\rm ex}$ and $B_{\rm ex}$ exhibit anomalous behavior at $r_s\approx 9.51$. Because $B_{\rm ex}$ is much decreased at $r_s\approx 9.51$ and becomes smaller further for $r_s>9.51$, the effect of this singularity on $\varepsilon^R(\boldsymbol{q},\omega)$ is gradually enhanced with the increase of r_s.

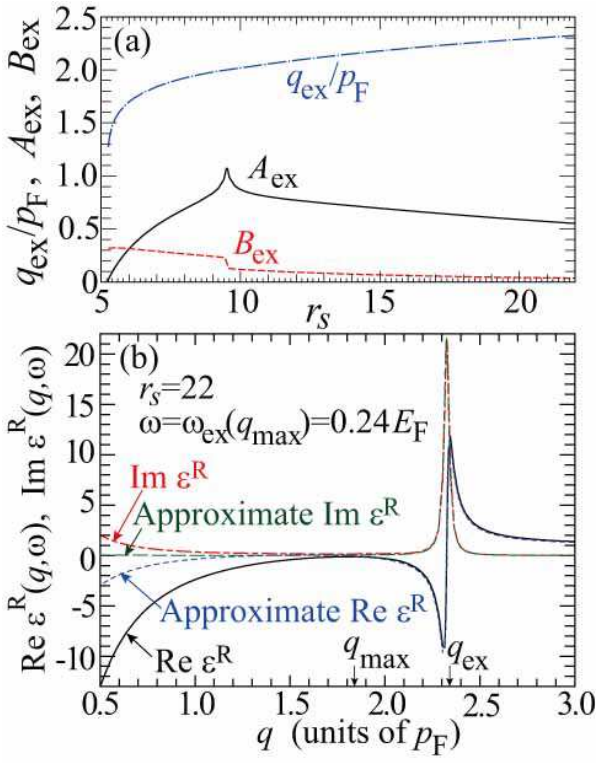

FIG. 16: (Color online) (a) Calculated $q_{\rm ex}$ in units of $p_{\rm F}$, $A_{\rm ex}$, and $B_{\rm ex}$ as a function of r_s. (b) Comparison of $\varepsilon^R(q,\omega)$ between the full calculation in Eq. (53) and the approximate one in Eq. (71) at $r_s=22$ for $\omega=0.24E_{\rm F}$ at which energy $S(\boldsymbol{q},\omega)$ becomes maximum due to the excitonic collective mode.

In Fig. 16(b), we have given an example of the comparison between the approximate form for $\varepsilon^R(\boldsymbol{q},\omega)$ in Eq. (71) and the full result of $\varepsilon^R(\boldsymbol{q},\omega)$ in Eq. (53) calculated at $r_s=22$, from which we can confirm the accuracy of this approximate form in the neighborhood of the singular point at $(q,\omega)=(q_{\rm ex},0)$. This figure also shows that the excitonic-peak position providing the maximum height in $S(\boldsymbol{q},\omega)$, $(q_{\rm max},\omega_{\rm ex}(q_{\rm max}))$, is actually coincident with the point in (q,ω) space at which $\varepsilon^R(\boldsymbol{q},\omega)\approx 0$, validating to call $\omega_{\rm ex}(q)$ "the excitonic collective mode". In this way, the excitonic collective mode is brought about by the singular behavior of $\varepsilon^R(\boldsymbol{q},\omega)$ associated with the singularity at $(q_{\rm ex},0)$ which is originally induced by the ghost exciton mode.

Finally in Fig. 17, $\varepsilon^R(\boldsymbol{q},\omega)$ given in Eq. (53) is plotted at $r_s=22$ in the whole (q,ω) space in order to fully represent the typical behavior of $\varepsilon^R(\boldsymbol{q},\omega)$ in the dielectric-catastrophe regime. As a general feature, $\varepsilon^R(\boldsymbol{q},\omega)$ contains a couple of singular points. Associated with each singularity, there appears a collective mode at which $\varepsilon^R(\boldsymbol{q},\omega)\approx 0$, leading to the double-peak structure in

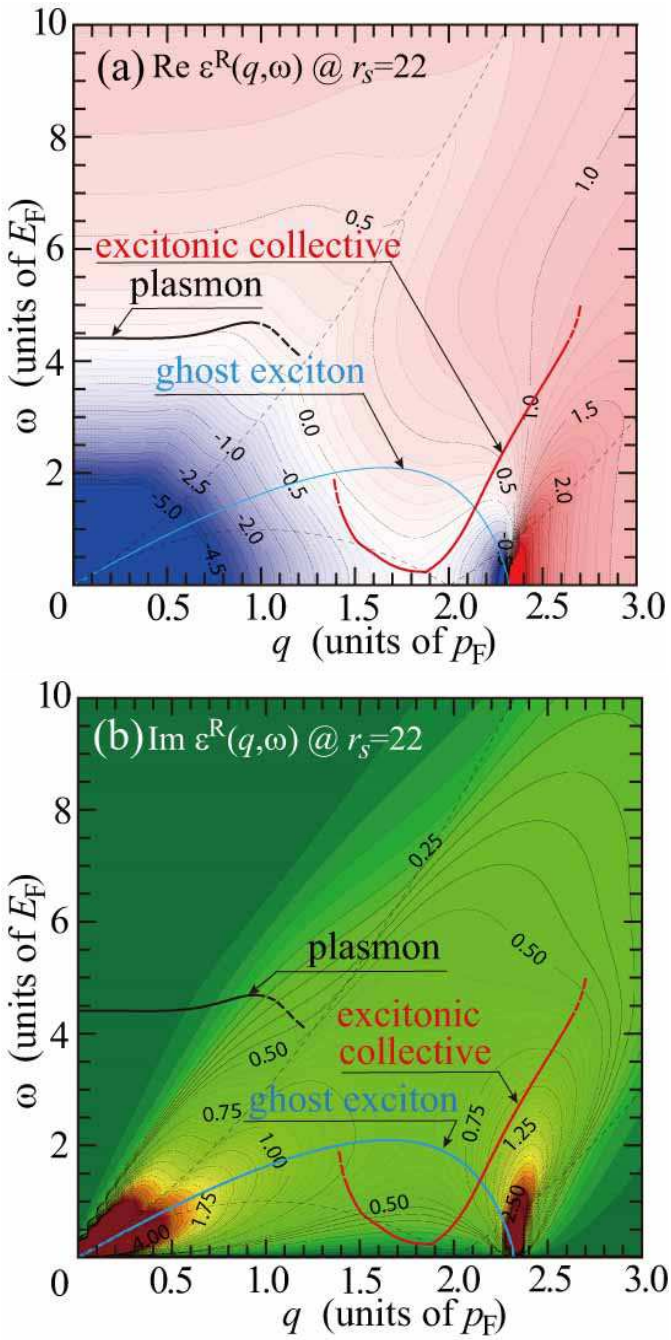

FIG. 17: (Color online) Two-dimensional contour map of $\varepsilon^R(\boldsymbol{q},\omega)$ at $r_s = 22$ for (a) real and (b) imaginary parts.

$S(\boldsymbol{q},\omega)$, one for the plasmon and the other for the excitonic collective mode, as shown in Fig. 1(b).

IV. CONCLUSION AND DISCUSSION

In this paper, we have calculated the momentum distribution function $n(\boldsymbol{p})$ and the dynamical structure factor $S(\boldsymbol{q},\omega)$ in the three-dimensional (3D) electron gas at low densities, i.e., $r_s > 5.25$, in which the electronic compressibility κ is negative. The obtained $n(\boldsymbol{p})$ is considered to be sufficiently accurate, because it rigorously satisfies not only the exact asymptotic behavior but also the three sum rules, Eqs. (3)-(5), the last of which is successfully derived in this work. The obtained $S(\boldsymbol{q},\omega)$ is also considered to be sufficiently accurate, because the two ingredients to construct $S(\boldsymbol{q},\omega)$, namely, $\Pi^R_{\rm WI}(\boldsymbol{q},\omega)$ and $G^R_s(\boldsymbol{q},\omega)$, are both reliably determined in accordance with all the known constraints that must be fulfilled for correct evaluation of those quantities. For $r_s > 10$, the calculated $S(\boldsymbol{q},\omega)$ exhibits a peak structure due to the excitonic collective mode in addition to the well-known plasmon peak. With the increase of r_s, this new peak structure grows steadily and eventually for $r_s > 20$ it dominates the plasmon peak. Associated with this excitonic collective mode, a singularity is found for the first time in $\varepsilon^R(\boldsymbol{q},\omega)$ at $q \approx 2p_{\rm F}$ and $\omega = 0$, which is the direct physical consequence of the appearance of the ghost exciton mode for $r_s > 5.25$.

Four comments are in order:

(i) Although we have treated the 3D electron gas in this paper, exactly the same physics will be found in the 2D electron gas in which the dielectric catastrophe regime appears for $r_s > 2$. Actually, negative κ has already been observed in the 2D system.[50,51] Thus, in order to confirm the emergence of the excitonic collective mode by the measurement of $S(\boldsymbol{q},\omega)$ in some suitably designed experiments, the 2D system may be more recommended, although detailed calculation for the 2D system is left for the future.

(ii) Physically, if the excitonic collective mode is a dominant polarization process in the charge response to an external point-charge perturbation, we may imagine that the screening effect will be much reduced than that in the usual metals due to the fact that the excitation of tightly-bound electron-hole pairs does not contribute to screening, indicating that the Hartree-Fock (HF) approximation may work well in the evaluation of some of physical quantities. This might be the reason why Ilani et al.[51] found that HF described their experimental results well in the metallic state at negative κ.

(iii) As mentioned in Secs. II F and III E, we find indications of some exotic electronic phase transition of the 3D electron gas for $r_s > 20$. We need to make a further study of the possibilities of such a phase transition, but at the same time, we need to take account of a possibility of partially spin-polarized state for $20 < r_s < 40$,[5] suggesting us to investigate the fate of the excitonic collective mode in the spin-polarized state as well as the coupling between charge and spin channels, a difficult but very intriguing problem left in the future.

(iv) Finally, we remark on similarity and difference between the plasma and the excitonic collective modes. Due to $\varepsilon^R(\boldsymbol{q},\omega) \approx 0$ at each mode in the relation of $\boldsymbol{D}(\boldsymbol{q},\omega) = \varepsilon^R(\boldsymbol{q},\omega)\boldsymbol{E}(\boldsymbol{q},\omega)$, there exists a wave-like charge-density oscillation as an eigenmode, accompanied by a finite elec-

tric field $\boldsymbol{E}(\boldsymbol{q},\omega)$ even in the absence of an external force (i.e., $\boldsymbol{D}(\boldsymbol{q},\omega)=\boldsymbol{E}(\boldsymbol{q},\omega)+4\pi\boldsymbol{P}(\boldsymbol{q},\omega)\approx 0$). The associated electric polarization $\boldsymbol{P}(\boldsymbol{q},\omega)$ is made of collective electron-hole excitations and works as a restoring force. Those charge-density oscillations can be quantized as bosons, just as the plasma oscillations quantized into the plasmons. In spite of those similarities, there is an important difference in the correlation among excited electrons and holes; for the plasmons, because its energy is larger than $E_{\rm F}$, all excited electrons and holes are uncorrelated, as can be well treated in RPA. For the excitonic collective modes, on the other hand, the excitations occur as a collection of excitons, indicating no polarization field in the long-wavelength limit and thus the absence of the mode at $|\boldsymbol{q}|\to 0$; the polarization appears, if $|\boldsymbol{q}|$ is of the order of $2p_{\rm F}$ or the inverse of the exciton binding radius. Incidentally, if we consider the exotic phase mentioned in (iii) in terms of a spontaneous excitation of this charge-density oscillation, it might be regarded as a CDW state in the sense of not nesting-driven but Overhauser[52,53].

Acknowledgments

This work is supported by a Grant-in-Aid on Innovative Area "Materials Design through Computics: Complex Correlation and Non-Equilibrium Dynamics" (No. 22104011) from the Ministry of Education, Culture, Sports, Science, and Technology, Japan.

* Email: takada@issp.u-tokyo.ac.jp: This paper will be published in Phys. Rev. B.

[1] See, for example, G. F. Giuliani and G. Vignale, *Quantum Theory of the Electron Liquids*, (University Press, Cambridge, 2005).
[2] D. M. Ceperley and B. J. Alder, Phys. Rev. Lett. **45**, 566 (1980).
[3] S. H. VoskoCL. WilkCand M. NusairCCan. J. Phys. **58**C 1200 (1980).
[4] J. P. Perdew and Y. Wang, Phys. Rev. B **45**, 13244 (1992).
[5] G. Ortiz, M. Harris, and P. Ballone, Phys. Rev. Lett. **82**, 5317 (1999).
[6] G. G. Spink, R. J. Needs, and N. D. Drummond, Phys. Rev. B **88**, 085121 (2013).
[7] G. Ortiz and P. Ballone, Phys. Rev. B **50**, 1391 (1994).
[8] M. Holzmann, B. Bernu, C. Pierleoni, J. McMinis, D. M. Ceperley, V. Olevano, and L. Delle Site, Phys. Rev. Lett. **107**, 110402 (2011).
[9] Y. Takada and H. Yasuhara, Phys. Rev. B **44**, 7879 (1991).
[10] H. Maebashi and Y. Takada, Phys. Rev. B **84**, 245134 (2011).
[11] See, for example, G. D. Mahan, *Many-Particle Physics*, 3rd edn. (Kluwer Academic/Plenum Press, New York, 2000), p. 355.
[12] Y. Takada, Phys. Rev. B **43**, 5979 (1991).
[13] D. Pines and P. Noziéres, *The Theory of Quantum Liquids*, (Benjamin, New York, 1966), Vol. 1.
[14] K. Matsuda, K. Tamura, and M. Inui, Phys. Rev. Lett. **98**, 096401 (2007).
[15] H. Maebashi and Y. Takada, J. Phys. Soc. Jpn. **78**, 053706 (2009).
[16] H. Maebashi and Y. Takada, J. Phys.: Condens. Matter **21** 064205 (2009).
[17] O. V. Dolgov, D. A. Kirzhnits, and E. G. Maksimov, Rev. Mod. Phys. **53**, 81 (1981).
[18] C. A. Kukkonen and A. W. Overhauser, Phys. Rev. B **20**, 550 (1979).
[19] Lack of knowledge on this structure of the effective electron-electron interaction erroneously leads to proposing various types of CDW instability; for example, A. M. J. Schakel, Phys. Rev. B **64**, 245101 (2001).
[20] Y. Takada, J. Superconductivity **18**, 785 (2005).
[21] K. Takayanagi and E. Lipparini, Phys. Rev. B **56**, 4872 (1997).
[22] Y. Takada, Phys. Rev. Lett. **87**, 226402 (2001).
[23] J. C. Ward, Phys. Rev. **78**, 182 (1950).
[24] Y. Takahashi, Nuovo Cimento Ser.10 **6**, 370 (1957).
[25] Y. Takada and H. Yasuhara, Phys. Rev. Lett. **89**, 216402 (2002).
[26] Y. Takada, Molecular Phys. **114**, 1041 (2016).
[27] P. Gori-Giorgi and P. Ziesche, Phys. Rev. B **66**, 235116 (2002).
[28] C. F. Richardson and N. W. Ashcroft, Phys. Rev. B **50**, 8170 (1994).
[29] M. Lein, E. K. U. Gross, and J. P. Perdew, Phys. Rev. B **61**, 13431 (2000).
[30] See, for example, Y. Takada, Phys. Rev. B **47**, 3482 (1993).
[31] J. C. Kimball, J. Phys. A: Math. Gen. **8**, 1513 (1975).
[32] H. Yasuhara, Solid State Commun. **11**, 1481 (1972).
[33] H. Yasuhara, J. Phys. Soc. Jpn. **36**, 361 (1974).
[34] A. W. Overhauser, Can. J. Phys. **73**, 683 (1995).
[35] P. Gori-Giorgi and J. P. Perdew, Phys. Rev. B **64**, 155102 (2001).
[36] S. Moroni, D. M. Ceperley, and G. Senatore, Phys. Rev. Lett. **75**, 689 (1995).
[37] G. NiklassonCPhys. Rev. B **10**, 3052 (1974).
[38] I. O. Kulik, Zh. Éksp. Teor. Fiz. **40**, 1343 (1961) [Sov. Phys. JETP **13**, 946 (1961)].
[39] E. K. U. Gross and W. Kohn, Phys. Rev. Lett. **55**, 2850 (1985); **57**, 923(E) (1986).
[40] B. DabrowskiCPhys. Rev. B **34**, 4989 (1986).
[41] N. Iwamoto and E. K. U. Gross, Phys. Rev. B **35**, 3003 (1987).
[42] A. Holas and K. S. Singwi, Phys. Rev. B **40**, 158 (1989).
[43] R. Nifosì, S. Conti, and M. P. Tosi, Phys. Rev. B **58**, 12758 (1998).
[44] Z. Qian and G. Vignale, Phys. Rev. B **65**, 235121 (2002).
[45] K. MorawetzCPhys. Rev. B **66**, 075125 (2002).
[46] L. A. Constantin and J. M. Pitarke, Phys. Rev. B **75**, 245127 (2007).
[47] R. D. Puff, Phys. Rev. **137**, A406 (1965).
[48] K. N. Pathak and P. Vashishta, Phys. Rev. B **7**, 3649 (1973).
[49] N. Iwamoto, Phys. Rev. A **30**, 3289 (1984).
[50] J. P. Eisenstein, L. N. Pfeiffer, and K. W. West, Phys. Rev. Lett. **68**, 674 (1992); Phys. Rev. B **50**, 1760 (1994).

[51] S. Ilani, A. Yacoby, D. Mahalu, and H. Shtrikman, Phys. Rev. Lett. **84**, 3133 (2000); Science **292**, 1354 (2001).
[52] A. W. Overhauser, Phys. Rev. bf 128, 1437 (1962); **167**, 691 (1968): Adv. Phys. **27**, 343 (1978).
[53] J. P. Perdew and T. Datta, phys, stat. sol. (b) **102**, 283 (1980); H. T. Tran and J. P. Perdew, Am. J. Phys. **71**, 1048 (2003).